DYNAMIC FAILURE PROPERTIES OF THE PORCINE MEDIAL COLLATERAL LIGAMENT: PREDICTING HUMAN INJURY IN HIGH SPEED FRONTAL AUTOMOTIVE COLLISIONS

By

Louis Raymond Peck

A Thesis

Submitted to the Faculty of the Worcester Polytechnic Institute

In Partial Fulfillment of the Requirements for the

Degree of Master of Science

In

Mechanical Engineering

May 2007

Approved:

_____	_____
Prof. Malcolm Ray	Prof. Kristen Billiar
Advisor	Committee Member
_____	_____
Prof. Mark Richman	Prof. Yiming Rong
Committee Member	Graduate Committee Representative

Abstract

Twenty five porcine knee collateral ligaments were tested to determine the dynamic failure properties of ligaments. A test fixture, to be placed in a drop tower, was designed to apply an axial impulsive impact load to a porcine bone-ligament-bone complex. The applied strain rates ranged from $0.005s^{-1}$ to $145s^{-1}$. The data from the impact tests was analyzed using the method of linear regression to construct predictive model equations capable of forecasting the failure load and failure stress of a ligament subjected to a specific strain rate. 73% of the ligaments tested failed via tibial avulsion while the remaining ligaments failed via mid-substance tearing. The failure: load, strain and stress all increased with the applied strain rate. Further an interesting correlation between geometric ratios, namely the initial length divided by the initial cross sectional area and vice versa, and the failure load and stress were identified. Using this information, model equations were developed that predict the failure stresses based on the load and strain rate. The motivation for this study was to develop failure properties that could be used in an LSDYNA finite element model of the human lower extremities based on the understanding that the properties of porcine knee collateral ligaments would be similar to human ligaments. The properties developed in this study can be used to estimate the human response in high speed frontal automotive collisions.

Acknowledgements

I would like to sincerely thank my advisor, Professor Malcolm Ray, for his guidance, support and the opportunity to work on such an interesting and exciting project. I would also like to thank Don Pellegrino for the countless hours he donated to help me out and make sure the project was a success. Much of this project would not have been possible without Don's advice and suggestions. Further, I would like to thank both Malcolm Ray and Don Pellegrino for their seemingly unconditional faith in my ability to accomplish the goals of the project. Thanks also to Kristen Billiar for his invaluable advice and direction. Without Professor Billiar's input this project couldn't have reached the level of quality it has. Additionally, I would like to gratefully acknowledge the National Highway Traffic Safety Administration for supporting this research and the University of Massachusetts Medical School, and Sue Wheeler, for donating the porcine organs necessary to conduct this research.

Personally, I would like to thank my friends and family for their support and understanding throughout my academic career. I would also like express my appreciation to Ellen Lynch, for the many sacrifices she has made so I may accomplish my academic ambitions.

Table of Contents

List of Figures

List of Tables

Nomenclature

A_o	Initial cross sectional area of ligament at mid-substance (mm)
E	Modulus of elasticity
$\varepsilon_{failure}$	Grip to grip strain at the point of failure (%)
ε_{rate}	The grip to grip strain rate at the point of failure (s^{-1})
η	Coefficient of viscosity
L_o	Initial stress-free free length of ligament (mm)
MS	Mid-substance failure
P_F	Load at the point of failure (N)
R^2	Coefficient of determination
σ_F	Load at the point of failure divided by A_o (MPa)
TA	Tibial avulsion
V_{imp}	Velocity of the drop tower hammer at the point of impact (m/s)
W_o	Initial width of the ligament at mid-substance (mm)

1. Introduction

Occupants involved in high speed frontal automotive collisions are often victims of knee, hip and thigh (KTH) injuries. These injuries commonly result in long term or permanent disabilities with high societal costs. In fact, the cost of KTH related injuries caused by frontal automotive collisions is approximately four billion dollars per year [1]. In order to prevent KTH injuries in high speed frontal automotive collisions, it is imperative understand the biomechanics and failure characteristics of the KTH and all of its components, including ligaments.

The objective of this study is to determine the failure properties of KTH ligaments subjected to impact conditions presented in high speed frontal automotive collisions. This will be accomplished by performing uni-axial impact tests on the medial collateral ligament of the porcine knee, abbreviated MCL. The information obtained in this study will be integrated into a finite element analysis simulation program to predict the injury potential of occupants in high speed frontal automotive collisions.

Animal knees were used for testing in this study due to the difficulties of procuring human organs in sufficient quantities. Further, porcine knees were selected because it has been shown, when modeling human behavior, that the porcine knee is the favored model for experimental studies when compared to other animals [2].

Additionally, the MCL and the LCL were used for testing due to the fact that the knee is responsible for more injuries in the KTH complex than any other component [1]. Also, these ligaments are relatively easy to extract. For reference, Figures 1.1 and 1.2 show photographs of porcine and human knees respectively.

Figure 1.1: Photograph of porcine knee

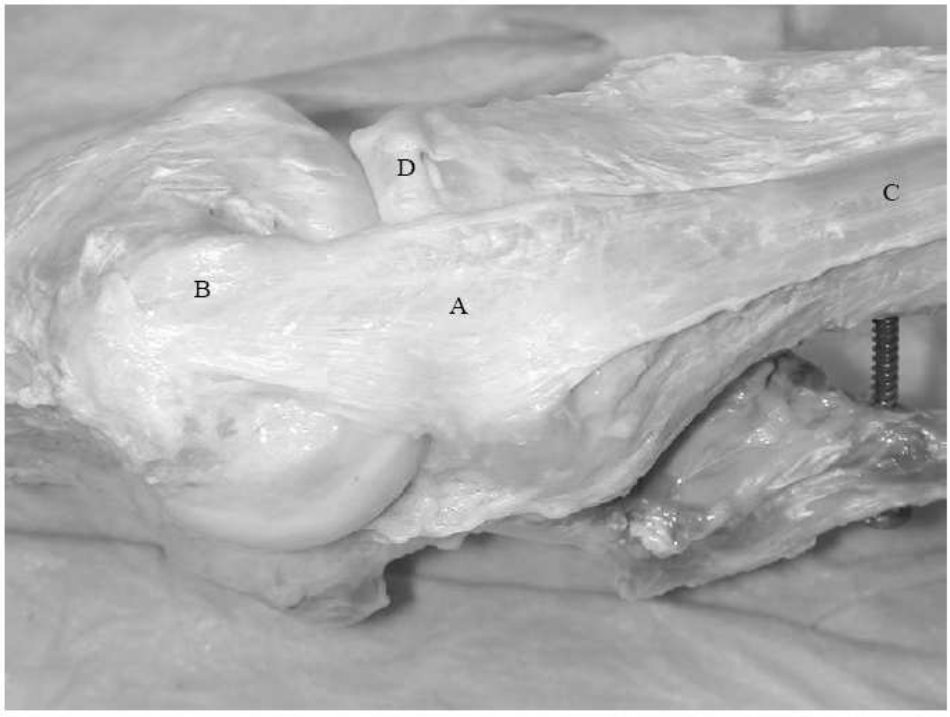

Figure 1.2: Photograph of human knee: (A) MCL (B) origin (C) insertion and (D) meniscus [3]

It is well known that ligaments demonstrate viscoelastic behavior and the material properties are therefore rate dependant [4]. Consequently, it is possible that the failure properties of ligaments also depend on the rate at which the load is applied. Therefore, ligaments were tested at a variety of extension rates consistent with conditions presented in high speed frontal automotive collisions.

Many studies have been performed in attempt to understand ligament failure mechanics and to quantify the failure properties [4-7]. However, because of the difficulties inherent to high speed impact testing, few of the previous studies properly address the extension rates present in high speed frontal automotive collisions. Further, none of the prior studies utilized animals that may accurately represent human behavior.

2. Methods

According to studies performed to quantify knee and hip velocities of properly restrained occupants in frontal automotive collisions, the knee and hip peak velocities, relative to the vehicle's interior, are 33% and 35% of the vehicle's change in velocity, respectively [8]. Using this fact and common velocity changes for high speed frontal automotive collisions, it was determined that the ligaments in this study should be tested using extension rates ranging from 1.5m/s to 6.0m/s.

In order to accurately determine the failure characteristics of the MCL and LCL, the entire bone-ligament-bone complex was tested. This ensures that the ligament origin and insertion sites are included in the study, and also eradicates problems presented when attempting to directly grip a viscoelastic material.

To represent the conditions presented in high speed frontal collisions as accurately as possible the ligament will be subjected to impulsive impact loads. Also, to isolate the longitudinal properties, the impact force placed on the ligament will be oriented axially.

2.1 Fixture Design

In order to test the porcine ligaments under the conditions mentioned above, it was necessary to design a testing fixture. The design of this fixture was based largely on the concepts of an initial design, created by students of Worcester Polytechnic Institute working with the National Highway Traffic Safety Administration (NHTSA) (see Figure 2.1). Figure 2.1 shows the initial design. When a load is applied to the top disk of the fixture, a tensile force of the same magnitude is placed on the specimen in the fixture. To subject the specimen to the extension rates detailed above, this fixture will be placed in a Dynatup 8250 Drop Tower (see Figure 2.2). This drop tower has a maximum drop height of 46 inches as well as a pneumatic assist option to achieve high velocity impacts. The hammer of this tower will strike the top disk of the test fixture, subsequently loading the test specimen.

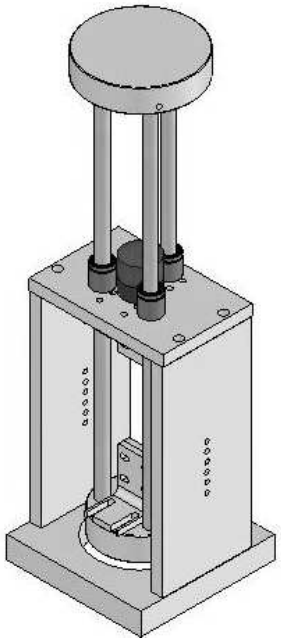

Figure 2.1: Initial ligament fixture design

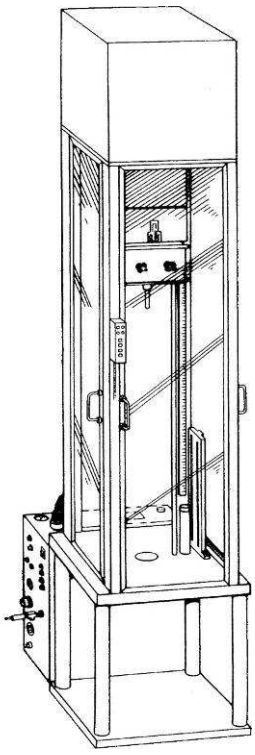

Figure 2.2: Instron Dynatup 8250 drop tower ©

There were three major issues that needed to be addressed when designing the second generation test fixture. These issues included: ligament gripping, data acquisition and fixture usability and efficiency.

The original design gripped the ligament between two plates, which were secured together by four bolts. This method significantly reduced the cross sectional area of the ligament, creating artificial high stress concentrations which lead to unnatural failures.

The most prominent issue with the initial design was its inability to collect the data required for analysis. The goal was to have the ability to record the axial load placed on the specimen and the rate at which this load was applied. The original fixture design had no incorporated instrumentation. The only data available, therefore, was from the load cell located on the drop tower hammer. Preliminary testing, using high speed video, showed the drop tower hammer was not in constant contact with the

test fixture and could not, therefore, provide accurate feedback relative to the specimen loading. This finding lead to the understanding that instrumentation must be incorporated in the design of the fixture allowing a direct measurement of the force placed on the specimen as well as the acceleration, speed and position of the moving parts of the fixture.

Finally, the initial design was difficult to use and consequently inefficient. The original design made it very complicated and time consuming to insert a test specimen. Each grip, top and bottom, had four nut and bolt assemblies to secure, which were hard to access as a result of the three bearing rods surrounding the grips (see Figure 2.1). This access problem made it necessary to remove the test fixture from the drop tower each time a new specimen was to be loaded.

Another issue, relative to usability and efficiency, was the inability to hold a specific tare load on the specimen. There were only two preloading conditions possible when using the initial design. The specimen could either be preloaded by the mass of the moving parts of the fixture, or be relieved of all loading by inserting thin wooden dowels into the fixture, consequently supporting the weight of the moving parts. These dowels would support this weight until the hammer of the drop tower struck the fixture. At this point the wooden dowel would break, therefore allowing the specimen to be subjected to the impact loading. However, there were a limited number of locations for the wooden dowel to be placed, which in turn limited the flexibility of the initial loading conditions.

All of these issues were resolved in the second generation design. The second generation fixture was designed using a three dimensional modeling program with stress analysis capabilities. Figure 2.3 shows a rendering of the second generation design.

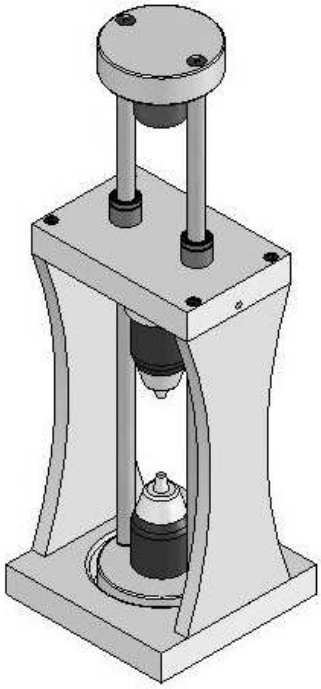

Figure 2.3: Second generation ligament fixture design

The grip issue was initially resolved by incorporating a three jaw, keyless chuck. Several bench tests showed the chuck had equal holding power when compared to the original design, and did not reduce the cross sectional area of the specimen as severely. Later, it was determined the best method to test ligaments would be to incorporate the bone. The bones could be easily modified to fit in the gripping chuck and would eliminate the high stress concentrations associated with gripping the ligament directly. Also, including the bone in the test allows additional valuable data to be obtained; namely, the behavior of the ligament-bone junction, a common failure site under certain strain rate conditions.

Figure 2.4: Photograph of gripping method using brackets

Figure 2.4 shows the final gripping configuration utilized. It can be seen that two quarter inch bolts were inserted, transversely, through the femur and tibia or fibula. These bolts were secured to the chucks using a u-shaped bracket. This method proved to be more efficient and effective when compared to directly gripping the bone with the three jaw chuck and also enabled quick installation and removal of test specimens.

The data acquisition problems were solved by integrating an accelerometer and a load cell in the design of the fixture. Figure 2.5 shows the location of both components.

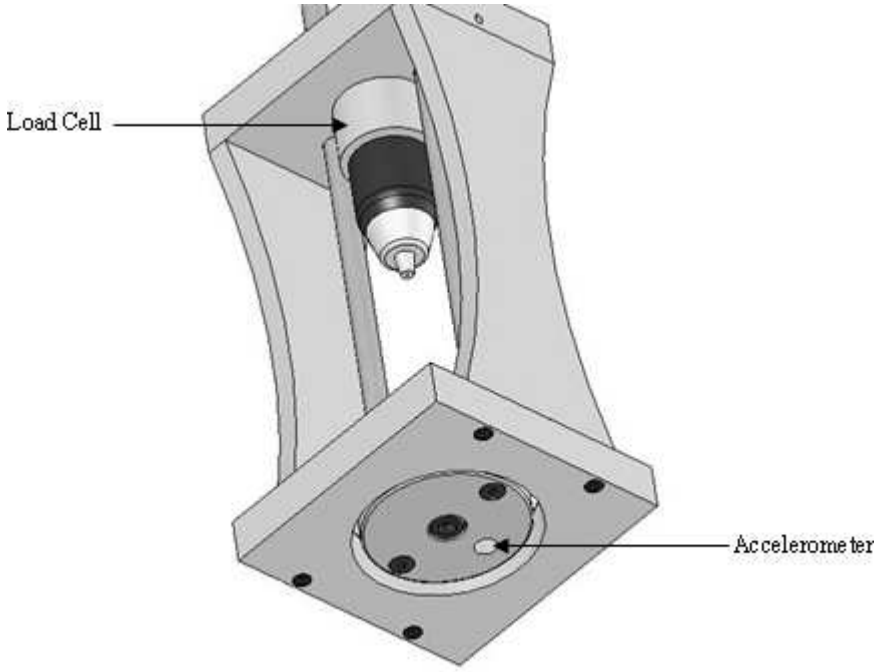

Figure 2.5: Rendering showing the location of the load cell and accelerometer

As can be seen in Figure 2.5, the gripping chuck is threaded on the load cell allowing a direct readout of the specimen axial force. Knowing the cross sectional area of the specimen and this axial force, the tensile stress can be calculated. Figure 2.5 also shows the placement of the accelerometer. This accelerometer recorded the instantaneous acceleration and allowed the speed and position of the fixture's moving parts to be calculated at any moment (see Appendix A for a complete list of the equipment used). The information gathered from the accelerometer and load cell enabled stress versus grip-to-grip strain rate relationships to be developed.

Several changes were made to improve the specimen installation process. One of these changes involved the bearing rods. Only two rods were used, instead of the original three rod configuration, allowing greater access to the grips. Stress and buckling analyses were conducted using SolidWorks, Cosmos and standard engineering principles, to ensure this modification would not lead to any loss of

structural integrity (see Figure 2.6, Appendix B). A change was also made to the side supports of the fixture to allow for greater access. Instead of a straight edge, an arc was used. Again, the proper analyses were performed to ensure this change would not affect the strength of the fixture (see Appendix B).

Finally, instead of using wooden dowels to set the tare load prior to testing, nylon tipped set screws were used (See Figure 2.6). These nylon tipped set screws were placed in the top plate of the fixture, on both sides, enabling them to contact the bearing rods. The coefficient of static friction between the steel rods and the nylon was determined to be adequate to set reasonable tare loads with little pressure. Once the drop tower hammer struck the fixture, the coefficient of static friction was broken and the coefficient of dynamic friction was the only force resisting movement. This force is negligible when compared to the forces of interest. The tips of the set screws were nylon to ensure no rod scarring would occur.

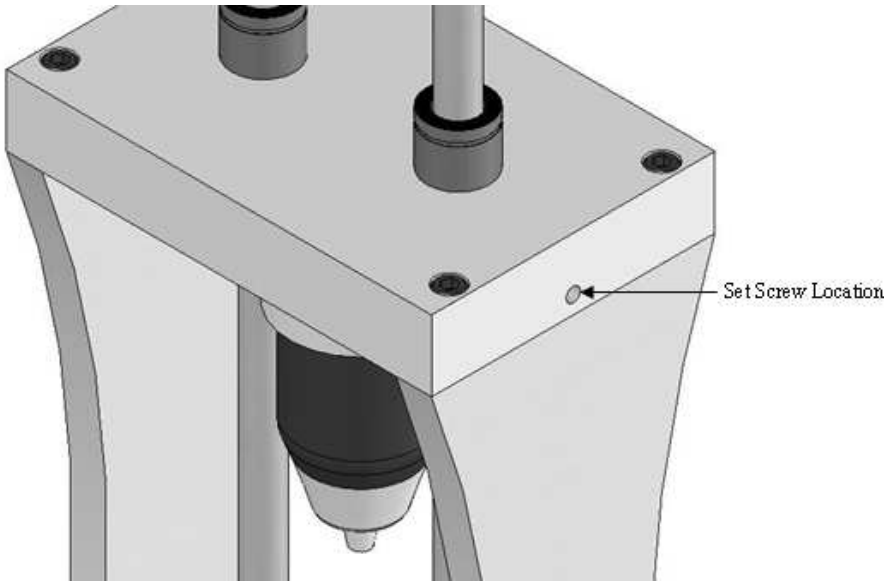

Figure 2.6: Rendering showing the location of the nylon tipped set screws

All of the above additions, changes and modifications created an easier to use, more efficient and effective testing device. Figure 2.7 shows a photograph of the finished design.

Figure 2.7: Photograph of the ligament test fixture final design

2.2 Testing

The testing process consisted of three phases: verification of the instrumentation, impact testing of leather straps for method validation, and impact testing of mature porcine ligaments.

2.2.1 Verification of Instrumentation

Several tests were conducted to verify the data acquisition instrumentation. To verify the load cell, a number of masses were weighed using a calibrated scale. These masses were then weighed using the load cell and the results were compared. The weights spanned the loading range expected during live testing and the measurements were performed at the sampling frequency that will be used during live testing to ensure validity. This information, in conjunction with the calibration sheet provided by the

load cell manufacturer, provided sufficient evidence to prove the data produced by the device was valid.

The accelerometer was verified using two processes. The first process involved translating the acceleration measurements into information regarding the fixture's position using simple properties of linear dynamics, namely unidirectional double integration. Specifically, two measurements were taken on the fixture, the initial position and the position at which the moving parts of the fixture reach a stopping point. This distance was compared to the distance recorded by the accelerometer.

The accelerometer data was also verified using the concepts of conservation of momentum. The mass of the moving parts of the fixture and the drop tower were determined and recorded. Using the hammer impact speed, which is recorded by the drop tower data acquisition system, and an approximate coefficient of restitution determined using high speed video, the theoretical post impact speed of the fixture's moving components was calculated. This number was compared to the value calculated using the acceleration data gathered from the accelerometer. Similar to the load cell, a calibration sheet was also provided by the manufacturer.

2.2.2 Leather Straps

Once the instrumentation was validated, impact testing of leather laces was performed. These tests were conducted to test all of the equipment and to develop a method for data processing. Perfecting the testing process with leather straps ensured fewer mistakes would be made when testing porcine ligaments. The following is a detailed description of the leather testing process.

Leather shoe laces were used for these tests, specifically tan Kiwi® outdoor boot laces. These laces were cut into three inch lengths the day of testing. An inch and a half length was then measured and marked on the specimen. This measurement represents the initial, stress-free length of the specimen, which is required to determine the strain rate during impact. The cross sectional area of the middle portion of the lace was then measured using calipers and recorded. This specimen was then loaded in the fixture. The grips were tightened so the chucks gripped the leather directly on the marks indicating the stress-free-length of the specimen. All of the equipment was then configured to record the impact data at 20 KHz. The drop tower hammer was raised to the appropriate height, or in the case when a pneumatic assist was needed, the air pressure regulator was set to the correct pressure. The hammer was then released. This was repeated many times, and the data from these tests was recorded. Once it was certain the above procedure was mastered, porcine ligaments were tested.

2.2.3 Porcine Ligaments

Mature porcine knees were obtained from two sources: a local slaughterhouse, Lemay and Son's Beef Co., Inc., and the University of Massachusetts Medical School. The knees were frozen the day of termination at -20° Celsius in Ziploc® Double Guard® freezer bags with surrounding tissue in tact. Studies have shown the biomechanical properties of ligaments, when stored using a similar method, do not differ significantly from those of fresh samples [9]. The knees were thawed the day of testing in a bath of water at room temperature and were tested within one month of initial storage.

After thawing, both the MCL and the LCL were extracted for testing. To do this the patella was removed and the knee was cut in half, longitudinally, using a pneumatic reciprocating saw. At this point, half of the knee was put aside and wrapped in saline soaked gauze (0.9% NaCl) while the other half was being prepared. Further, the meniscus and the fascia surrounding the ligament were removed.

It is very important to remove excess fascia from the ligament to ensure the strain markers are adhered directly to the ligament. If the strain markers are placed on fascia surrounding the ligament, the markers will move independently of the ligament and, therefore, will not be fit for the local strain analysis using high speed video. Additionally, excess fascia can cause inaccurate cross sectional measurements of the ligament. The ligament was frequently misted with saline solution during preparation to maintain hydration.

To prepare the specimen for gripping, two pilot holes were drilled for the gripping bolts. These holes were drilled in the femur and tibia or fibula, depending on which ligament was being tested. The holes were positioned at optimal locations to ensure the specimen was loaded axially (see Figure 2.4). If these holes were not positioned properly the load would not be oriented axially and the ligament would be prone to undesirable tearing at the site of origin and insertion. The stress-free initial length of the ligament was measured using dial calipers at this point. The length used for the ligament initial length was determined by measuring the free length. Neither the insertion or origin areas were included in this measurement. Optimally, this dimension would have been recorded once the tare load was applied to the specimen, but gripping conditions prevented any accurate measurement of the ligament length at this point. Therefore, the measurement was taken before the grips were installed.

The gripping mechanisms were then installed and the ligament-bone complex was placed in a quasi-static tensile testing machine. A tare load of approximately 20 N was placed on the ligament and the mid-substance cross sectional dimensions were measured. The area was assumed to be rectangular, therefore the mid-substance width and thickness were the only cross sectional dimensions recorded. The specimen was then pre-conditioned to 7% of the initial stress-free, free length of the ligament at a

rate of 0.25 mm/s. The ligament was preconditioned to simulate *in vivo* conditions as accurately as possible.

The specimen was then loaded into the impact test fixture. Three strain markers, equally spaced and centered about the mid-substance, were place on the ligament. Graphite flakes were used for these markers and were attached to the ligament approximately 2 minutes prior to testing using cyanoacrylate, also known as high viscosity super glue.

Finally, the high speed video system was configured to record the test at 2000 frames per second and the test was conducted. The load cell and accelerometer data acquisition rate for these tests was 25 KHz.

Three porcine knees received were unacceptable for impact testing. Two of the knees were too large to be testing in the impact fixture, and the third knee was received with lacerated ligaments caused during extraction of the knee. Since the knees could not be used for impact testing, they were used to gather information regarding the geometric parameters of the ligaments. These knees were prepared in a similar manner as the knees described above. However, before the gripping mechanism was attached, the cross sectional dimensions, at the mid-substance, and the initial length of the ligament were recorded. The ligament was then torn from both the site of origin and insertion. At this point, the approximate area of the ligament attachment sites was measured. The mid-substance cross sectional dimensions of the ligament were then compared to the area of the attachment sites to determine if any relationship existed which may help understand the ligament failure mechanics.

2.3 Analysis

As previously mentioned, the speed and position of the moving parts of the fixture must be determined to calculate the grip-to-grip strain rate, which is simply the extension rate at failure divided by the ligament initial length. An accelerometer was used to collect the data needed to determine these values. However, to obtain these values from the accelerometer, the data needed to be processed. In this case, because only axial speed and position are relevant, unidirectional single and double integration were used. These methods use acceleration-time histories to determine the speed and position of the moving parts of the fixture at any moment.

To ensure proper zeroing of the instruments, the zero calibration was performed in the post processing analysis spreadsheet. The first one thousand samples were set as pre-test values. The data from these points were averaged and this value was then subtracted from every future value.

Next, the failure point was located. This point was defined as the maximum force preceding any substantial decline in load. Using the information generated by the load cell and the accelerometer, the extension rate, load, and position at failure were identified and recorded. Again, the information needed from this data is strain rate and failure stress. The failure load was divided by the cross sectional area of the ligament to obtain the failure stress and the extension rate at failure was divided by the initial free length of the ligament to obtain the strain rate at failure. The grip-to-grip strain at failure was also calculated and recorded. This value was determined by considering the position change of the lower grip of the fixture and the initial free length of the specimen.

It is generally understood that the local strain, in biological materials, differs significantly from the grip-to-grip strain. Other researches have found that the grip-to-grip strain generally overestimates the

local strain by 150 - 200% [4]. The local strain of several specimens was verified using high speed video analysis tools to verify this finding. The strain markers were tracked manually, frame to frame, using Photron's® Motion Tools software package and the results were compared to the grip-to-grip strain measured by the fixture accelerometer.

The data obtained during testing was analyzed using SAS® version 9.1.2 and Mathematica® version 4.1. Specifically, regression and analysis of variance (ANOVA) techniques were utilized. Numerous iterations were executed in the pursuit of determining reliable predictors of the ligament failure load and stress. Many factors were used as independent variables including: the supplier of the porcine organ, the initial area of the ligament, the initial length of the ligament, the hammer impact velocity and the strain rate of the ligament. Additionally, physically significant ratios of these variables were analyzed.

For example, two very important predictive ratios were derived from Hooke's law, namely A_o/L_o and L_o/A_o. Hooke's law is simply:

$$(2.1)\quad \sigma = E\varepsilon$$

Equation 2.1 can be reformulated as follows:

$$(2.2)\quad \varepsilon = \frac{\sigma}{E} = \frac{P}{AE}$$

Recognizing that $\delta = \varepsilon L$ and substituting this into Equation 2.2 yields:

$$(2.3)\quad \delta = \frac{PL}{AE}$$

Solving this equation for P yields:

$$(2.4)\quad P = \frac{AE\delta}{L}$$

Since the ratio A/L is a geometric parameter that affects P, the ratio A_o/L_o was used as a predictor of the failure load when performing the statistical analysis. Similarly the ratio L_o/A_o was used as a predictor of the failure stress.

Attempts were also made to predict the failure stress using many variations of the Cowper-Symonds model. This constitutive equation is used to predict the yield stress of a material at a specific strain rate when the quasi-static yield stress of the material is known. The following variations of the Cowper-Symonds equation were used for analysis, where b, c and p are constants.

$$\sigma = \sigma_o \left(1 + \left(\frac{\varepsilon_{rate}}{c} \right)^{\frac{1}{p}} \right) \tag{2.5}$$

$$\sigma = \sigma_o \left(b\frac{L_o}{A_o} + \left(\frac{\varepsilon_{rate}}{c} \right)^{\frac{1}{p}} \right) \tag{2.6}$$

$$\sigma = \sigma_o \left(1 + \left(\frac{\varepsilon_{rate}}{c} \right)^{\frac{1}{p}} \right) + b\frac{L_o}{A_o} \tag{2.7}$$

$$\sigma = \sigma_o \left(1 + \left(\frac{\varepsilon_{rate} + \frac{L_o}{A_o}}{c} \right)^{\frac{1}{p}} \right) \tag{2.8}$$

3. Results

During testing it was found that gripping the LCL to allow for axial loading was extremely difficult due to the size and orientation of the fibula. Consequently, the following impact testing results are solely for the porcine MCL. However, a previous study examining the behavior of rat collateral ligaments found the biomechanical properties of the MCL and LCL are similar [10]. Therefore, it is believed that the information obtained during testing is valid with respect to the LCL as well as the MCL. Table 3.1 shows a summary of the results for impact testing. Note, several tests conducted were deemed unacceptable for analysis. The results for these tests can be found in Appendix C.

Table 3.1: Summary of results of impact tensile tests of porcine ligaments

ID	A_o (mm^2)	L_o (mm)	W_o (mm)	V_{imp} (m/s)	$\varepsilon_{failure}$ (%)	ε_{rate} (s^{-1})	P_F (N)	σ_F (MPa)	Failure Mode
1	6.10	36.96	3.56	2.27	31	63	521	86	MS
2	13.46	32.26	4.14	3.50	52	104	839	62	MS
3	6.74	38.39	4.57	4.67	27	138	600	89	MS
4	7.84	39.32	5.51	1.93	21	56	401	51	TA
5	12.31	32.51	5.98	2.00	31	61	768	62	TA
6	8.12	34.67	3.85	2.91	17	97	384	47	TA
7	11.21	36.73	4.01	3.83	30	119	786	70	TA
8	11.90	31.00	6.19	4.01	37	140	844	71	TA
9	20.08	26.67	7.23	UNK	48	145	1184	59	TA
10	15.18	38.52	4.57	UNK	25	137	600	40	TA
11	9.85	41.38	5.97	4.92	36	125	809	82	TA

Analyzing these results it is found that the mean failure stress, σ_F, is 65 MPa, the standard deviation of the population is 16 MPa and the 95% confidence level is ± 9.5 MPa. Similarly, the mean failure load, P_F, is 703N, the standard deviation is 232N and the 95% confidence level is ± 137N.

A quasi-static tensile test was conducted as well. The Table 3.2 shows the results.

Table 3.2: Results of quasi-static tensile test of porcine MCL

ID	A_o (mm^2)	L_o (mm)	$\varepsilon_{failure}$ (%)	ε_{rate} (s^{-1})	P_F (N)	σ_F (MPa)
12	42.57	50.93	69	0.005	2836	67

Table 3.3 shows a summary of results for the geometric relationship between the initial ligament mid-substance cross sectional area and the initial area of the ligament-bone attachment sites.

Table 3.3: Results of geometric relationship between mid-substance and attachment site for porcine collateral ligaments

Ligament	A_o (mm^2)	L_o (mm)	Origin A_o (mm^2)	Insertion A_o (mm^2)
MCL	9.2	44.7	1464.3	0.9
LCL	18.2	38.9	1703.2	
MCL	27.3	43.4	2851.6	0.9
MCL	27.7	39.6	2235.4	1.2
LCL	45.2	44.4	2296.7	

Table 3.4 shows a summary of results for the local strain analyses performed where G-G Strain is the grip-to-grip strain recorded and local strain is the strain recorded using high speed video and the strain markers previously described.

Table 3.4: Summary of results for local strain analysis

G-G Strain	Local Strain	Difference
31.0%	12.3%	252%
30.0%	0.0%	N/A
46.0%	0.0%	N/A
26.7%	-8.0%	-334%
29.2%	0.0%	N/A
47.7%	8.5%	561%

3.1 Mode of Failure

Table 3.1 shows that 73% of the failures were categorized as tibial avulsions. This mode of failure involved the ligament tearing from the insertion site of the tibia and was further characterized by a layer of cortical bone, having a gritty texture, attached to the avulsed end of the ligament [6]. These failures generally involved the detachment of a portion of the muscle surrounding the insertion site as well. A photograph of a typical tibial avulsion can be seen in Figure 3.1.

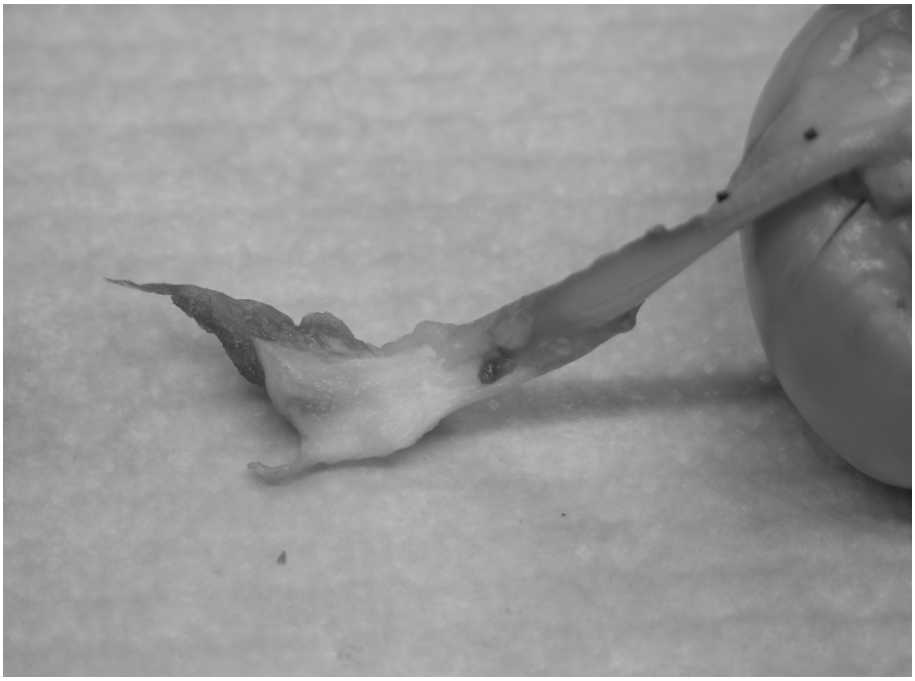

Figure 3.1: Photograph of porcine MCL tibial avulsion

While the majority of the ligaments failed via tibial avulsion, a significant portion of the failures, 27%, were defined as mid-substance failures. During this failure the ligament tore near the mid-substance of the ligament and the origin and insertion sites appeared to be undamaged. These failures were seen over the entire range of strain rates tested. The result of a typical mid-substance failure can be seen in Figure 3.2.

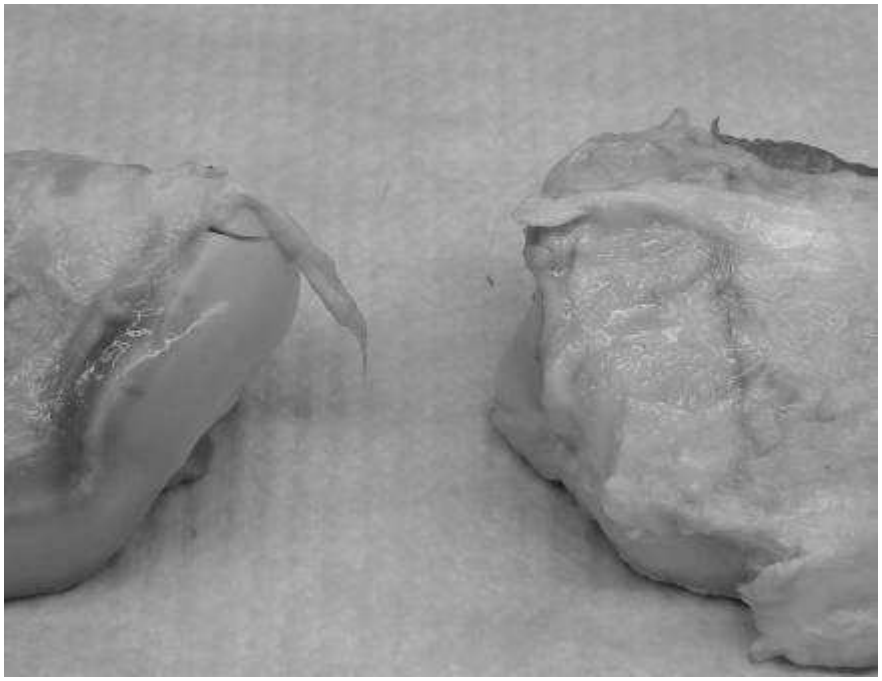

Figure 3.2: Photograph of porcine MCL mid-substance failure

3.2 Biomechanical Behavior

Figures 3.3 through 3.5 show the failure: load, stress and strain relative to the applied strain rate. Figure 3.3 shows that the failure load increases as the applied strain rate increases. No clear trend emerges when analyzing the failure stress with respect to the applied strain rate. It was necessary to perform statistical analyses to fully understand the relationship between these two variables. These analyses will be discussed in section 3.3. Figure 3.5 shows that the strain at failure, like the failure load, increases as the applied strain rate increases.

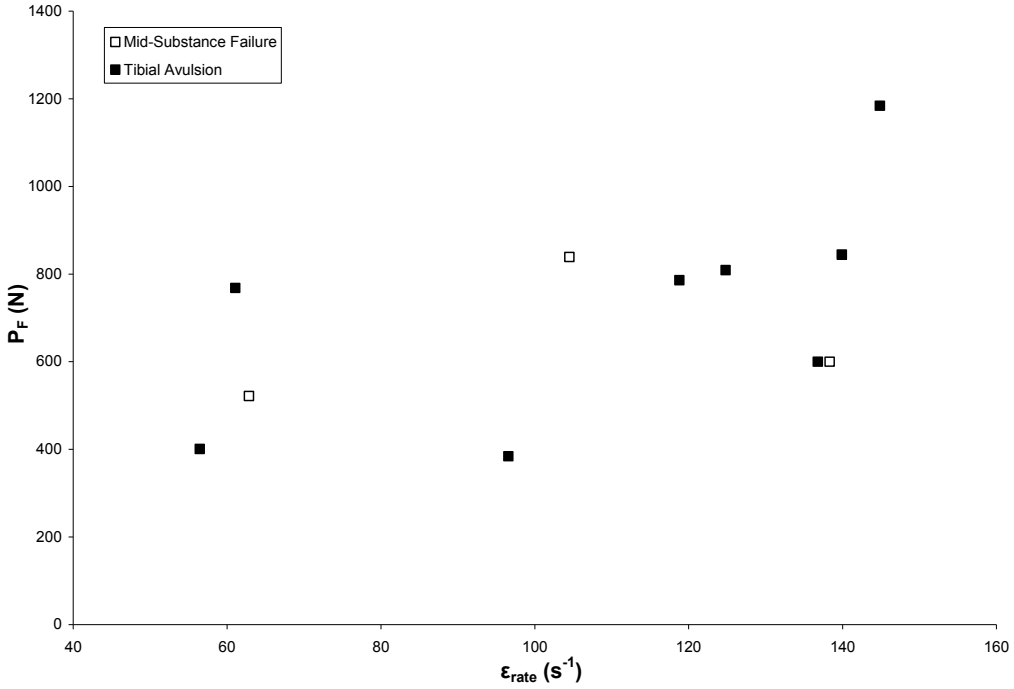

Figure 3.3: Failure Load v. Strain Rate for porcine MCL

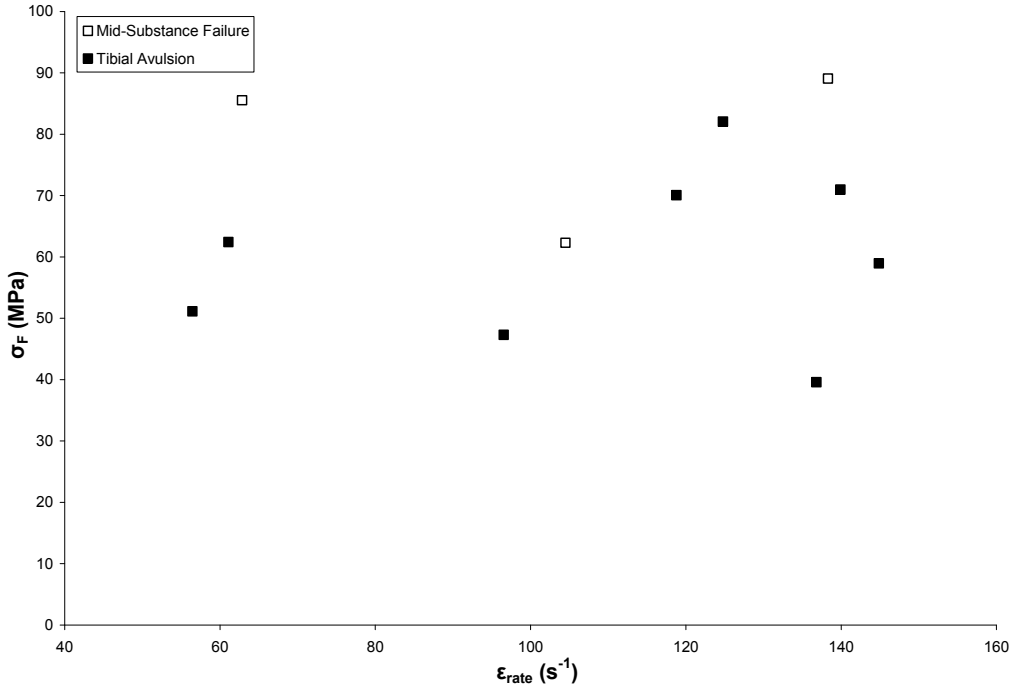

Figure 3.4: Failure Stress v. Strain Rate for porcine MCL

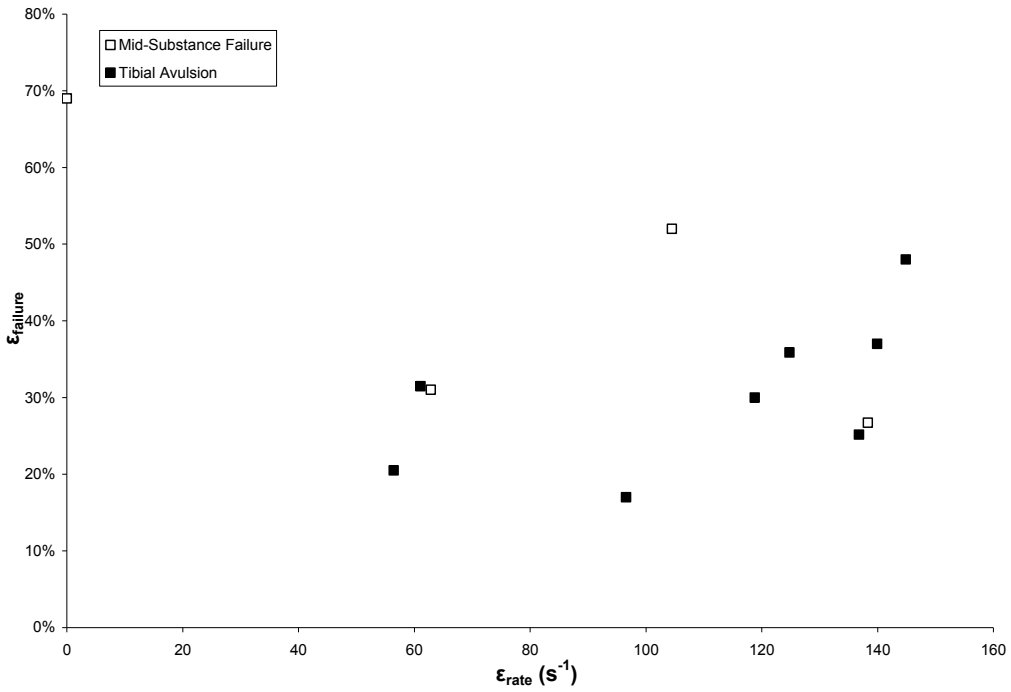

Figure 3.5: Failure Strain v. Strain Rate for porcine MCL

3.3 Statistical Analysis

As previously mentioned, statistical analyses were performed to find reliable predictors of the ligament failure load and stress. Table 3.4 shows the results obtained from the statistical analysis of linear models. The table shows the predictive variables, x_1, x_2 and x_3, the dependent variable, Y, the respective p-value for each variable and the R^2 value of the model. Identification (ID) numbers in the left column that have been bold faced are of special importance. Examining the analysis presented in bold face below it is seen that there are three reliable predictors of the failure load, namely: the initial cross sectional area, the applied strain rate and the ratio A_o/L_o. It is also seen that the failure strain correlates very well with the failure load, as expected. Two reliable predictors of the failure stress were also identified: the applied strain rate and the ratio L_o/A_o.

Table 3.4: Results of statistical analysis

ID	X_1	X_2	X_3	Y	P_1 Value	P_2 Value	P_3 Value	R^2
1	A_o			P_F	0.0001			0.9578
2	ε_{rate}			P_F	0.0001			0.9220
3	W_o			P_F	<0.0001			0.9469
4	Th_o			P_F	<0.0001			0.9028
5	Th_o			W_o	<0.0001			0.8614
6	L_o			P_F	<0.0001			0.8550
7	A_o			σ_F	0.0001			0.7832
8	L_o/A_o			σ_F	<0.0001			0.8949
9	L_o			σ_F	<0.0001			0.9456
10	$\varepsilon_{failure}$			σ_F	<0.0001			0.8935
11	A_o/L_o			P_F	<0.0001			0.9354
12	L_o/A_o			P_F	0.0016			0.6464
13	ε_{rate}			σ_F	<0.0001			0.8794
14	$\varepsilon_{failure}$			P_F	<0.0001			0.9727
15	$\varepsilon_{failure}$			σ_F	<0.0001			0.8935
16	ε^2_{rate}			σ_F	0.0002			0.7650
17	ε^2_{rate}			P_F	<0.001			0.8490
18	ε_{rate}	L_o/A_o		P_F	0.0003	0.8885		0.9221
19	ε_{rate}	L_o/A_o		σ_F	0.0032	0.0017		0.9620
20	ε_{rate}	A_o		σ_F	0.0249	0.8754		0.8797
21	ε_{rate}	L_o		σ_F	0.4570	0.0067		0.9490
22	ε_{rate}	A_o/L_o		P_F	0.0127	0.0051		0.9688
23	ε_{rate}	A_o/L_o		σ_F	0.0055	0.6881		0.8816
24	ε_{rate}	Th_o		P_F	0.0511	0.1649		0.9378
25	ε_{rate}	W_o		P_F	0.1329	0.0185		0.9592
26	ε_{rate}	A_o		P_F	0.1397	0.0064		0.9673
27	ε_{rate}	L_o		P_F	0.0178	0.5708		0.9248
28	ε^2_{rate}	L_o/A_o		σ_F	0.0073	0.0002		0.9548
29	ε^2_{rate}	A_o/L_o		P_F	0.0968	0.0018		0.9532
30	ε_{rate}	L_o/A_o	A_o	P_F	0.4072	0.5439	0.0085	0.9689
31	ε_{rate}	L_o/A_o	A_o	σ_F	0.2947	0.0023	0.4489	0.9648
32	ε_{rate}	L_o/A_o	Supplier	σ_F	0.4122	0.1062	0.6545	0.9663
33	ε_{rate}	L_o/A_o	V_{imp}	σ_F	0.9174	0.0235	0.4906	0.9749
34	ε_{rate}	L_o/A_o	F_{imp}	σ_F	0.0544	0.0082	0.9966	0.9599
35	ε_{rate}	L_o	A_o	P_F	0.3598	0.6994	0.0112	0.9679
36	ε_{rate}	A_o/L_o	Supplier	P_F	0.3772	0.0132	0.4458	0.9752
37	ε_{rate}	A_o/L_o	F_{imp}	P_F	0.8204	0.0168	0.2961	0.9680
38	ε_{rate}	A_o/L_o	V_{imp}	P_F	0.5289	0.3245	0.1883	0.9471

Further, the best combination of these predictors was identified to establish a predictive model. The best model was defined as the model with the lowest predictor variable p-values and the highest R^2 value. The model for the failure load consisted of a combination of the ratio A_o/L_o and the applied strain rate, while the model for the failure stress consisted of the ratio L_o/A_o and the applied strain rate. The resulting model equations are given below:

(3.1): $P_F = 3.0194\ \varepsilon_{rate} + 1091.5930\ A_o/L_o$

And

(3.2): $\sigma_F = 0.2888\ \varepsilon_{rate} + 9.2100\ L_o/A_o$

The results of the model equations are summarized in Tables 3.5 through 3.6. The root mean squared errors for the failure load and the failure stress are 224N and 16MPa respectively.

The p-values for the experimental variations of the Cowper-Symonds equations were far greater than 0.05. See Appendix D for detailed results of this analysis.

Table 3.5: Results of the model equation for the failure load

ε_{rate} (s^{-1})	P_F (N)	Predicted P_F (N)	Residual (N)
63	521	513	9
104	839	543	296
138	600	573	27
56	401	603	-202
61	768	633	135
97	384	664	-280
119	786	694	92
140	844	724	120
145	1184	754	430
137	600	784	-184
125	809	815	-6

Table 3.6: Results of the model equation for the failure stress

ε_{rate} (s^{-1})	σ_F (MPa)	Predicted σ_F (MPa)	Residual (Mpa)
63	86	74	12
104	62	52	10
138	89	92	-3
56	51	62	-11
61	62	42	20
97	47	67	-20
119	70	64	6
140	71	64	7
145	59	54	5
137	40	63	-23
125	82	75	7

Graphical displays of the results obtained from the model equations can be seen in Figures 3.6 through 3.9.

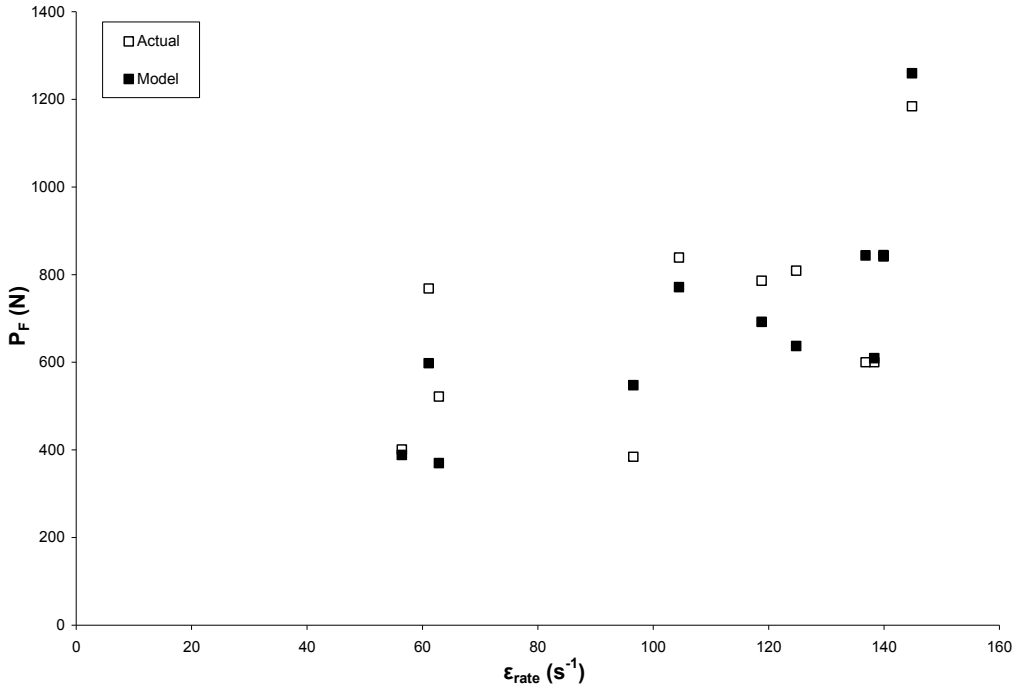

Figure 3.6: Actual Failure Load v. Model Failure Load for porcine MCL

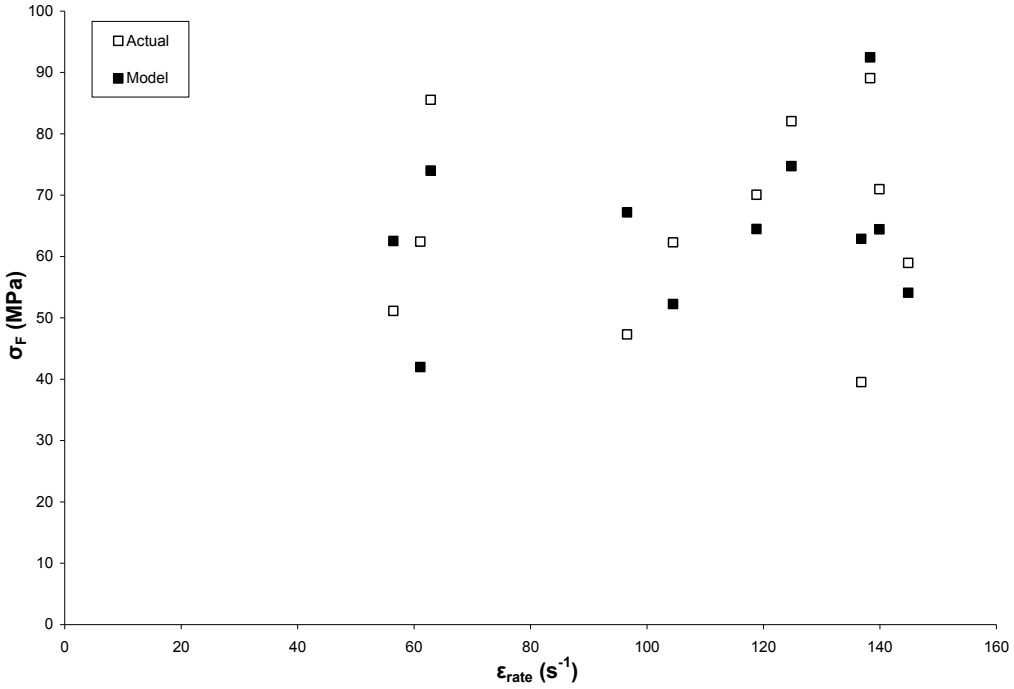

Figure 3.7: Actual Failure Stress v. Model Failure Stress for porcine MCL

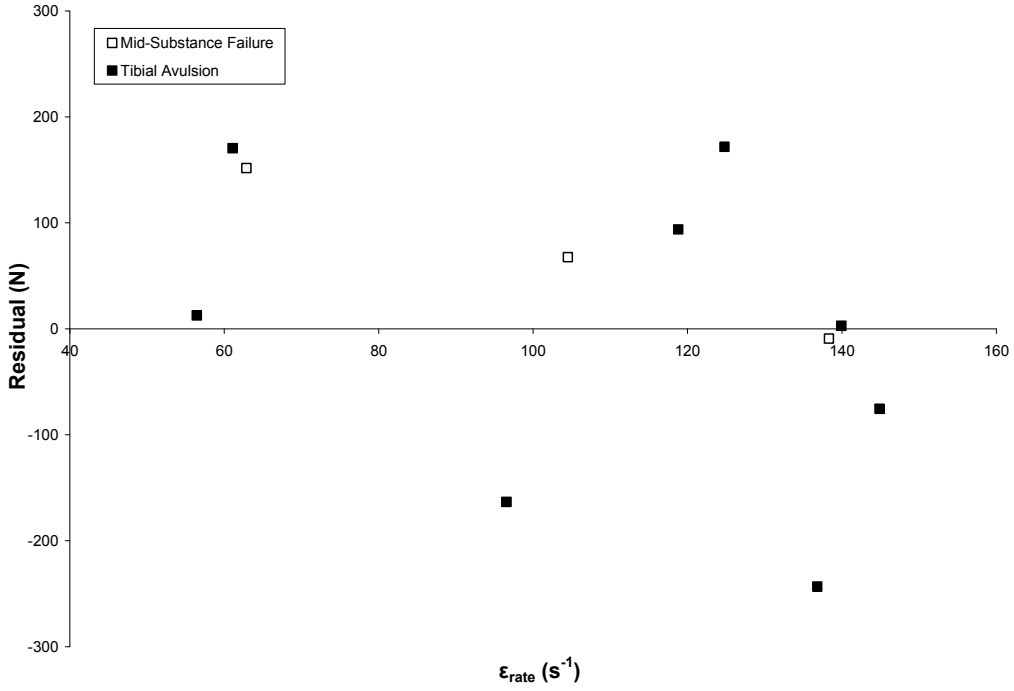

Figure 3.8: Failure Load Residual v. Strain Rate for porcine MCL model equation

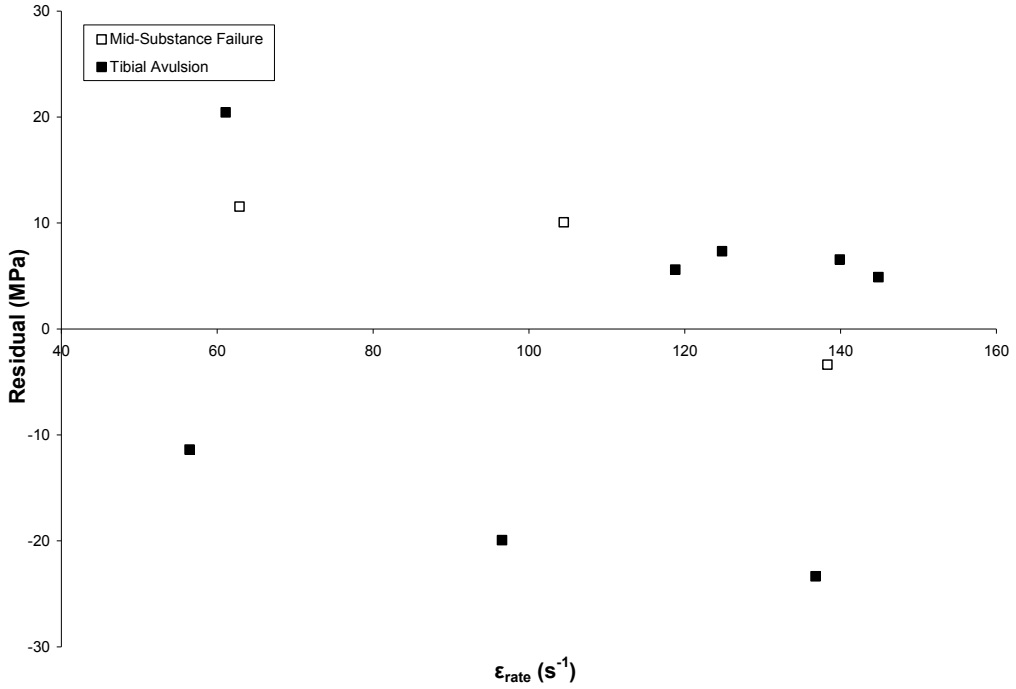

Figure 3.9: Failure Stress Residual v. Strain Rate for porcine MCL model equation

Figures 3.10 and 3.11 shows the results of the model equations for failure load and failure stress assuming the initial conditions of all the specimens are identical. Here, the mean ratio of A_o/L_o and L_o/A_o were used, these values were 0.33 and 3.6 respectively. This isolates the behavior of the failure load and the failure stress with respect to the strain rate, making it easy to see that they both increase as the strain rate increases. These figures also show the limits of the 95% confidence interval.

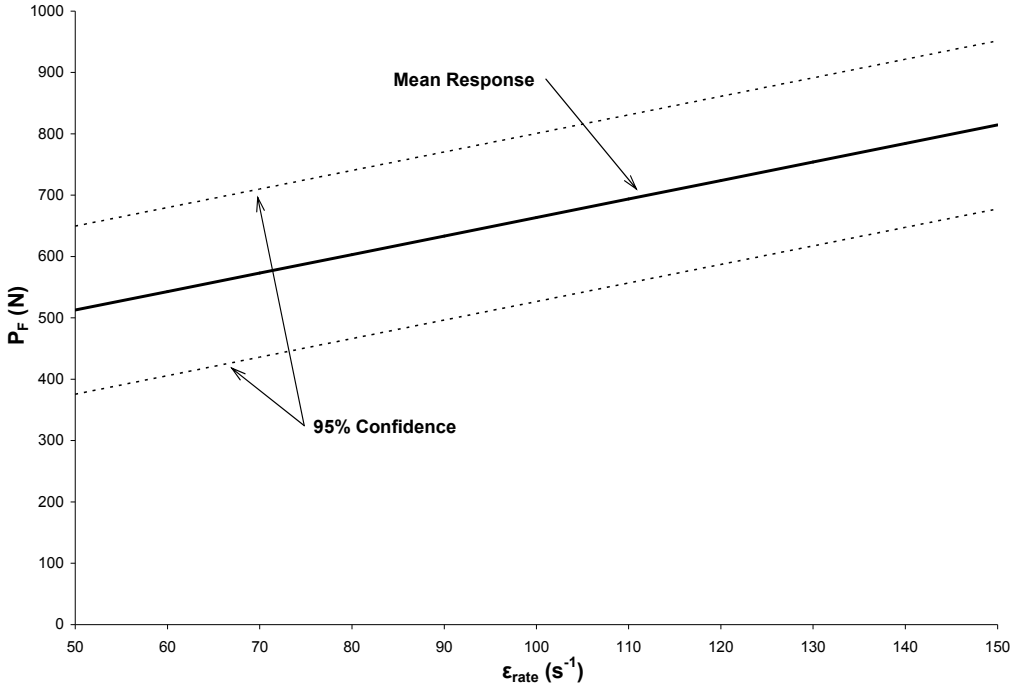

Figure 3.10: Predicted Failure Load v. Strain Rate of porcine MCL assuming uniform initial conditions

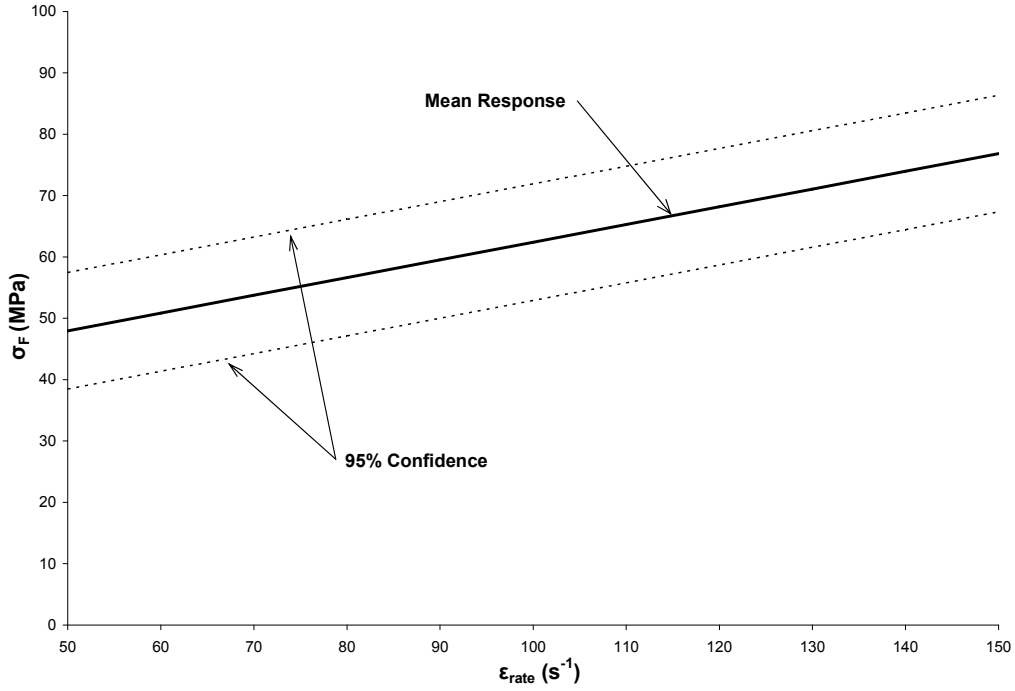

Figure 3.11: Predicted Failure Stress v. Strain Rate of porcine MCL assuming uniform initial conditions

Figure 3.12 and 3.13 show the relationships of failure load and failure stress and their corresponding predictive geometric ratios.

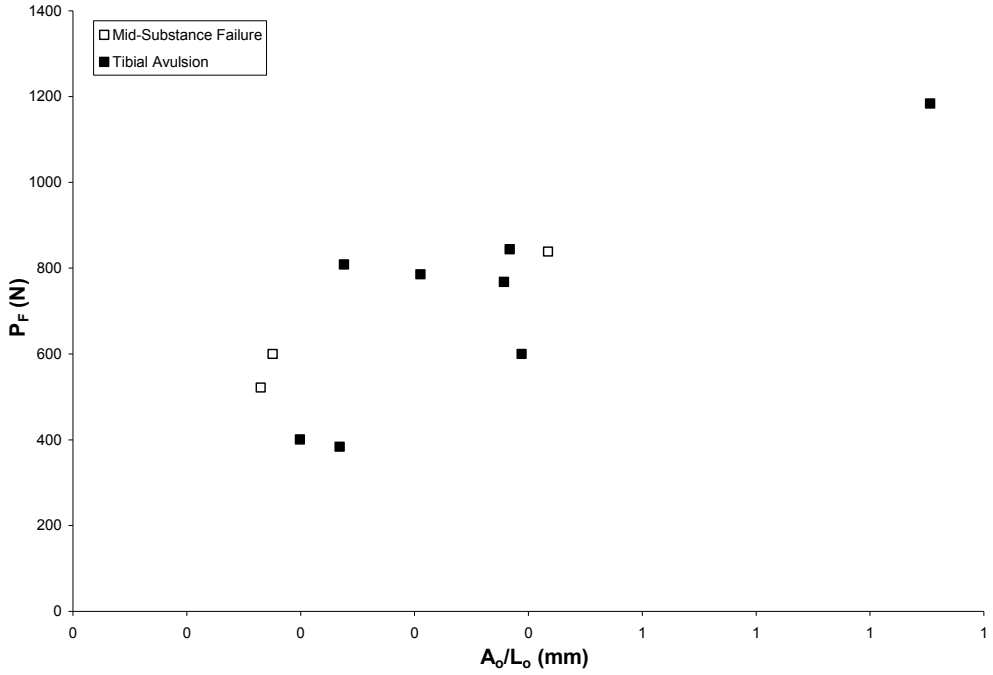

Figure 3.12: Failure Load v. A_o/L_o for porcine MCL

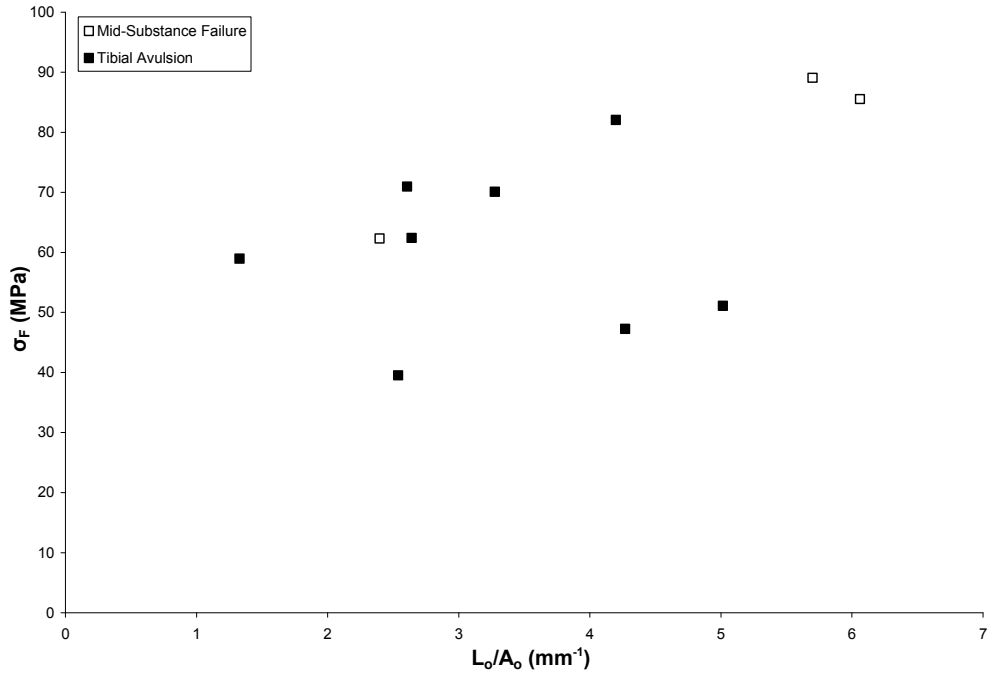

Figure 3.13: Failure Stress v. L_o/A_o for porcine MCL

The significance of the remaining graphs will be discussed in section 4.

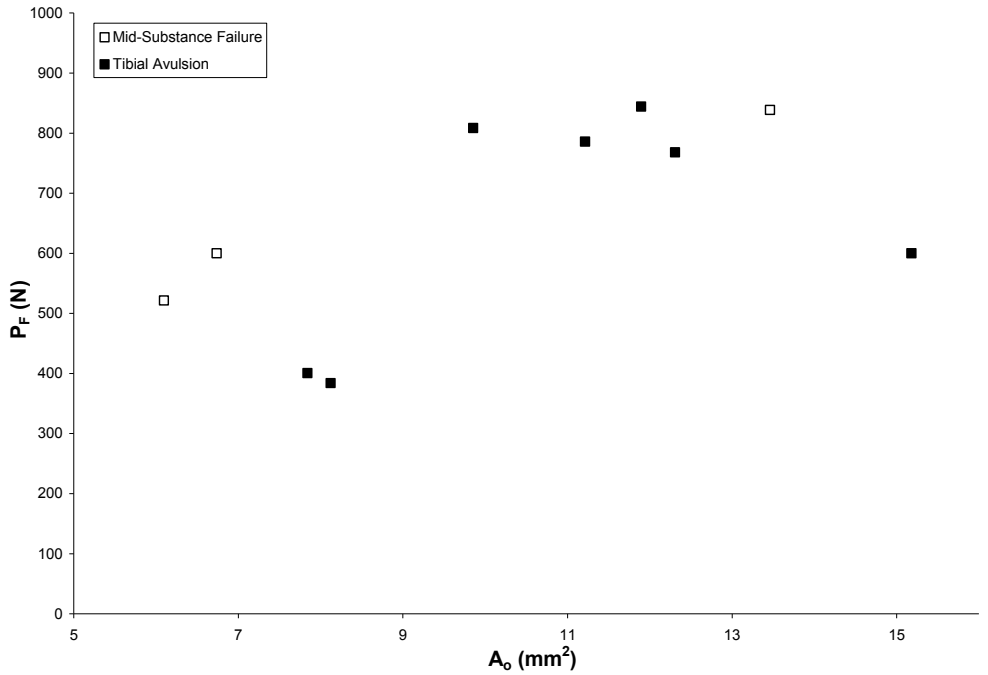

Figure 3.14: Failure Load v. Initial Cross Sectional Area for porcine MCL

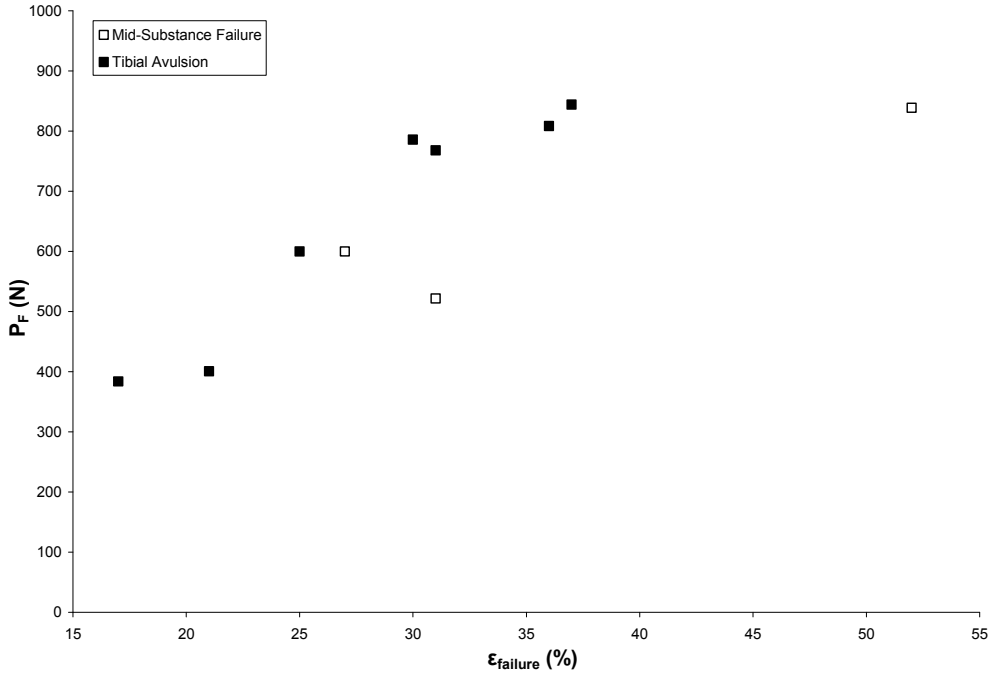

Figure 3.15: Failure Load v. Failure Strain for porcine MCL

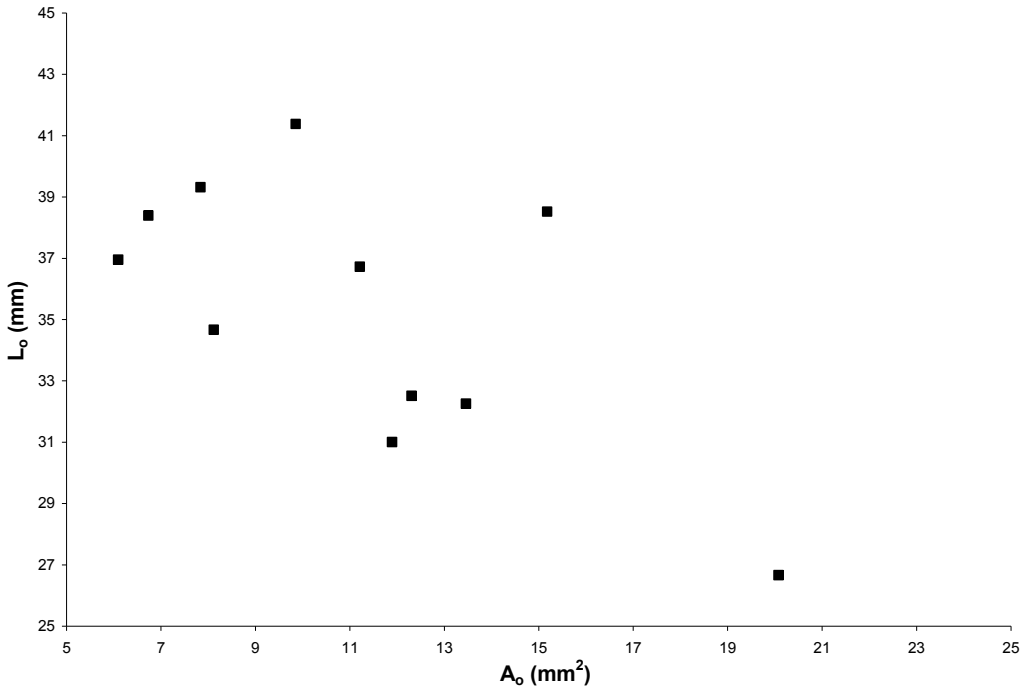

Figure 3.16: Initial Length v. Initial Area for porcine MCL

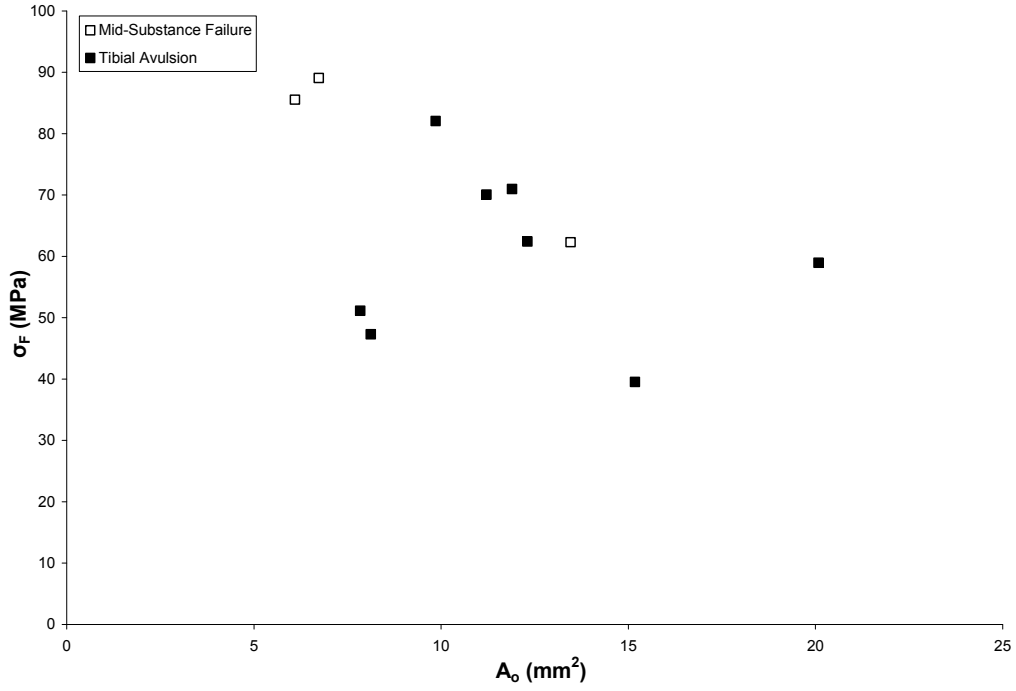

Figure 3.17: Failure Stress v. Initial Area for porcine MCL

4. Discussion

Twelve of the twenty five tests conducted were deemed unacceptable for analysis for many reasons including: improper loading conditions, improper gripping conditions and diseased specimens. See Appendix C for a complete summary.

4.1. Fixture Performance and Gripping Method

The test fixture designed for this study performed very well. The fixture enabled the acquisition of data necessary for analysis and showed no signs of damage after conducting hundreds of tests. However, there are two key modifications that could be made to optimize its performance and compatibility.

First, the stroke length should be increased to allow gripping of longer specimens. This would allow the researcher to place the gripping bolts further away from the ligament sites of origin and insertion. Secondly, the distance between the two bearing rods should be increased. This would allow testing of larger specimens such as large pig knees or human samples. However, the current design of the drop tower limits this width to approximately 5.7cm. Consequently, the configuration of the drop tower must be modified in order to make this change.

The gripping method proved to be successful when testing MCLs. However, the method was very ineffective for gripping ACLs due to the geometric parameters of the bone-ligament-bone complex of the femur-LCL-fibula. Unfortunately, the current study lends no recommendations to fix this problem.

4.2. Viscoelasticity

To properly discuss the results presented above it is necessary to discuss viscoelasticity. Ligaments, as well as almost all other biological materials, behave viscoelastically [11]. Viscoelastic materials exhibit both fluid and solid properties [11]. While hook's law: $\sigma = E\,\varepsilon$, is sufficient to explain the axial loading behavior of a linearly elastic material, the time dependant behavior of viscoelastic materials renders this equation inadequate. Consequently, a time dependant term must be included in this relationship. The stress-strain relationship for viscoelastic materials can be expressed as: $\sigma = f(\varepsilon, \varepsilon_{rate})$ [11]. The result of this relationship can be further understood by studying Figure 4.1 shown below.

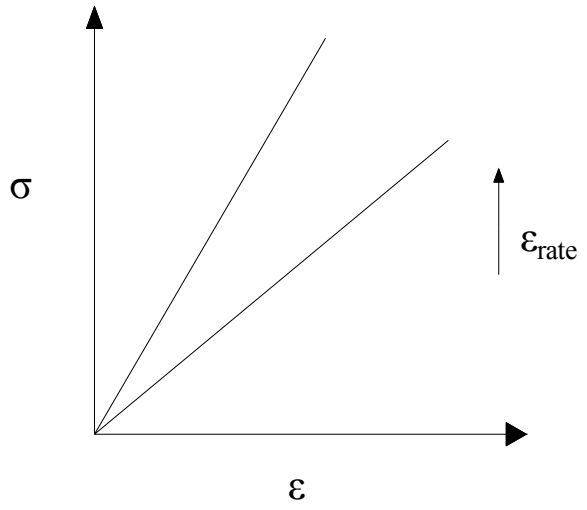

Figure 4.1: Stress, strain and strain rate relationship for viscoelastic material

Viscoelastic materials are modeled using a combination of a spring and a dashpot. Figure 4.2 shows a schematic of the Maxwell model which is commonly used to model the behavior of viscoelastic materials. The spring models the elastic behavior of the material, while the dashpot models the viscous behavior.

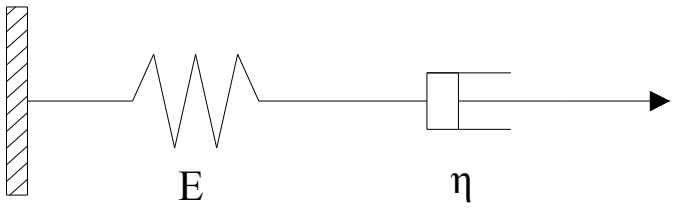

Figure 4.2: Maxwell model of viscoelastic materials

As Figure 4.1 shows, as the strain rate increases the stress level at a specific strain level will also increase. Similarly, the load at a specific strain will increase as the strain rate increases. These material properties are very important to remember when analyzing the results of this study.

4.3. Statistical Analysis

Many decisions made during the statistical analysis were influenced by the fact that the material being analyzed was viscoelastic. For example, it is known that the stress and loading characteristics of the viscoelastic materials, such as ligaments, depend on the applied strain rate. Consequently, it was understood that the applied strain rate likely had a strong level of correlation with respect to the failure load and the failure stress. Further, as shown above, ratios presented in Hooke's law were also used as predictors.

As expected the applied strain rate was a very reliable predictor of both the failure load and the failure stress. The ratios derived from Hooke's law also proved to be very reliable predictors of these two important failure properties (see IDs 2 and 13 in Table 3.4).

Studying Table 3.4 it is seen that the combination of these terms results in the best model. However, it is also seen that the initial cross sectional area of the ligament was a very reliable predictor of the

failure load and a moderately acceptable predictor of the failure stress (see IDs 1 and 7 in Table 3.4). However, equations 3.1 and 3.2 yield higher R^2 values and were therefore considered to be better equations to model ligament behavior.

The statistical results obtained from the Cowper-Symonds equations showed these equations do not accurately predict ligament behavior. As previously mentioned, the p-values for all of the experimental variations of the equation were far greater than 0.05. Consequently, the equations were discarded as possible predictive models.

4.4. Quasi-Static Tensile Testing

One quasi-static tensile test was performed. This test was run to obtain referential data to compare to the impact tests. It is interesting that the failure stress of the MCL tested quasi-statically does not differ from the results seen in the impact tests. Note, since the model is strictly used to model high strain rate failures, the quasi-static results were not used when generating the model equations for the impact tests.

4.5. Graphs

When analyzing the graphs in section 3 it is very important to remember that the cross sectional measurements were taken at the mid-substance of the ligament. Therefore, when the ligament fails via avulsion the stress presented is not the actual failure stress, but is instead the stress present at the mid-substance of the ligament at the point of failure. This method was implemented because of the difficulty presented when attempting to determine the cross sectional area of the avulsed region. Also note that the cross sectional area assumes the mid-substance of the ligament is rectangular.

Figure 3.3 shows that the failure load increases as the applied strain rate increases. When conducting tensile tests on human MCLs, France, *et al*, also found that the failure load increased as the applied strain rate increased [5].

Figure 3.15 shows that the failure load increases as the strain at failure increases. This result is expected, and can be understood by analyzing Hooke's Law, which shows that the stresswill increase as the strain increases.

Several previous studies have found that the failure stress increases as the applied strain rate increases [12-14], while Crisco found no significant difference in the failure stress of two groups tested at dramatically different strain rates [4]. Analyzing Figure 3.4 it appears there is no relationship between the applied strain rate and the failure stress. However, when other information is taken into account the relationship becomes clear. As previously mentioned, using statistical analysis it was found that the stress level where a ligament is likely to fail depends heavily on the ratio of its initial length over its initial area, or L_o/A_o. Analyzing this ratio and the applied strain rate simultaneously it is seen that the failure stress increases as the applied strain rate increases as found by the authors mentioned above (see Figure 3.11).

As discussed in section 2, linear regression analysis was used to find the relationship shown in Figure 3.11. This figure shows the model behavior of the failures stress as the applied strain rate increases assuming the initial conditions of all specimens are uniform. Graphing the failure stress using this method isolates the behavior of the failure stress with respect to the applied strain rate making it easy to see the relationship between these two important variables.

Figure 3.5 shows that the strain at failure increases as applied strain rate increases. Several other researchers have studied the affect of applied strain rate on the failure deformation of ligaments and have reported that the failure deformation either increased or remained the same as the applied strain rate increased [5, 7, 15, 16].

An interesting relationship is seen in Figure 3.13, which shows the failure stress with respect the ratio: L_o/A_o. It is seen that the failure stress increases as this ratio increases. In the case of failure via tibial avulsion, the relationship between this ratio and the failure stress exists because the failure load required to cause tibial avulsion generates a larger stress in ligaments with a smaller cross sectional area. Figure 3.17 confirms this finding. Further, the initial cross sectional area of the ligaments was found to decrease as the initial length increases, see Figure 3.16. Consequently, long and skinny ligaments experience larger stresses at the point of failure when compared to short and wide ligaments.

In the case of mid-substance failure this increase in failure stress is thought to be caused by the orientation and organization of the collagen fibers of the ligament. It is known that collagen fibers are responsible for the high tensile strength of ligaments [17]. Further, the collagen fibers are believed to be organized in bundles and oriented along the principle stress axis of the ligament. Therefore, depending on the geometry of the joint and ligament configuration, it is likely that not all collagen bundles are strictly parallel [17]. Taken these facts into consideration, it becomes clear that long and skinny ligaments may have highly organized and longitudinally oriented collagen fibers near the mid-substance due to the fact that the ligament is not required to provide support in any other direction at that location. On the contrary, the collagen fibers near the mid-substance of short and wide ligaments may be responsible for supporting loads in directions other than longitudinally, as a result of being

closer to the origin and insertion site, see Figure 4.3. Consequently, long and skinny ligaments may posses higher axial strength, which would describe the relationship shown in Figure 3.13.

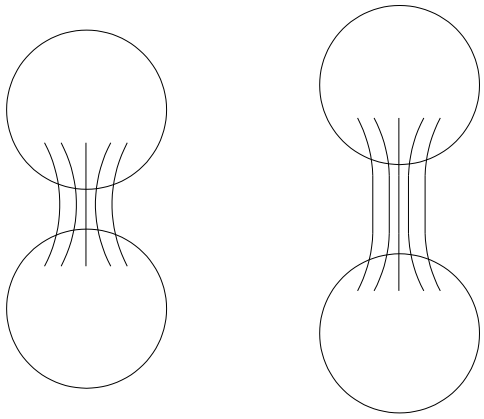

Figure 4.3: Possible orientation of collagen fibers in short and wide ligaments v. long and skinny ligaments

The aspect ratio of the ligament, or the ratio of the initial area compared to the initial length, also has a very important relationship to the failure load. The failure load increases as the ratio of A_o/L_o increases. This is likely due to the geometric conditions present at the sites of origin and insertion. Ligaments with larger cross sectional areas tend to have larger areas of origin, as seen in Table 3.3, and are therefore naturally stronger at this attachment site. It is believed that the same relationship is valid for the site of insertion. However, enough data was not gathered to validate this theory.

Figure 3.14 presents another piece of information pertinent to the governing dynamics of the failure load. This graph shows that the failure load increases as the initial cross sectional area of the ligament increases. This result is expected in the case of mid-substance failure and is consistent with the relationship between the failure load and the ratio A_o/L_o. It was thought that the initial cross sectional

area was the reason the ligament was stronger at the point of insertion. However, when only the cross sectional area of the specimen and the applied strain rate were used to predict the failure load, the model was not as accurate as the model which incorporated the ratio derived from the spring equation (see Table 3.4).

Figure 3.10 shows the model relationship between the failure load and the applied strain rate assuming uniform initial conditions. As discussed previously, graphing these variables using this method isolates the behavior of the failure load with respect to the applied strain rate, making it much easier to understand the relationship. The behavior seen in Figure 3.10 is consistent with the behavior of the failure load seen in Figure 3.3.

The performance of the model equations are shown in Figures 3.6 through 3.9. It is seen that both of the models seems to perform adequately and the residual plots are random and centered around zero indicating that there was no inherent errors in the testing method or results.

While the model predicts the failure stress moderately well, an argument could be made for defining a stress value with a level of confidence to predict the failure stress. For example, using the data presented it was found that the average failure stress was 65MPa. If the failure point for ligaments was defined as 65 ± 25MPa, this would be a possible method to predict the failure stress of ligaments. After all, Table 3.9 shows that the maximum residual failure stress is close to 25MPa. While this is a viable option, this method neglects the geometry of the ligament, consequently inhibiting the ability to extrapolate the results presented here for the MCL to other ligaments such as the ACL, LCL or hip ligaments.

4.6. Local Strain Analysis

Table 3.4 shows that the local strain analysis technique used was unsuccessful. Incomplete removal of excess fascia surrounding the ligament was most likely cause for this ineffectiveness. During preparation priority was given to the structural integrity of the ligament. Therefore, some fascia was not removed from the ligament to prevent ligamentous lacerations. However, in this study the local strain is not of special importance since the majority of failures were at or near the gripping points. Accordingly, the grip-to-grip strain rate is the measure of importance.

4.7. Mode of Failure

Previous studies have found that there are three possible ligament failure mechanisms: mid-substance tearing, ligament-bone interface failure such as avulsions, and tibial or femoral fracture [13, 18]. As shown above the two failure modes seen in this study were mid-substance failure and tibial avulsion, the majority of which were tibial avulsions. Lydon, *et al*, also found that the majority of failures were via tibial avulsion when testing the ACL of Rabbits [6]. Note, there are two possible categories of ligamentous avulsions. The ligament can either: tear from the insertion or origin site removing a conical portion of bone with it, or tear from the bone removing only cortical bone. The former is generally referred to as a bony avulsion while the latter is referred to as a fibrous avulsion. Not all studies report the type of avulsion seen, they merely report the fact that avulsion was the mode of failure. This must be considered when reviewing the literature.

While some researchers have found that tibial avulsion was the major cause of failure at low strain rates and mid-substance failure was the predominate mode of failure at high strain rates [15], the failure mode results of this study showed no strain rate dependence. This contradiction may be due to the fact

that the ligament failure mode depends on the type of ligament being tested because the viscoelastic properties of ligaments vary [19].

It is interesting to note that the results of the mid-substance failures mesh very well with the data from the tibial avulsions. This infers that the strength of the insertion site is similar, but weaker, than the strength of the mid-substance. It is also interesting that all of the avulsion failures occurred at the insertion site, indicating that the ligament-bone attachment at the tibia is weaker than the ligament-bone attachment of the femur. This is likely due to the fact that the insertion area is smaller than the origin area and consequently requires less force to cause the ligament to tear from the bone (see Table 3.3).

4.8. Extending MCL Results to Other KTH Ligaments

Since the model presented here considers the geometric properties of the ligament, it is possible to use the model equation to predict failure load and stress of ligaments other than the MCL. It is believed that the mid-substance failure stress of ligaments other than the MCL could be predicted moderately well using this model. However, considering the geometric differences of the origin and insertion sites between the MCL and many of the ligaments present in the KTH region it is thought that the model may be less accurate predicting avulsion failures. However, if the correlation between the ratios L_o/A_o or L_o/A_o and the failure stress and load are relevant to other ligaments, this model would prove to be very powerful. Further testing, using hip and cruciate ligaments from the knee, would have to be conducted to determine the significance of this model as it relates to other KTH ligaments.

4.9. Extending Porcine Results to Humans

As previously mentioned, it has been shown that the porcine knee, when compared to other animals, is the best model for experimental studies to predict human behavior [2]. Further, the size of many of the

porcine knees were similar to the size of human knees. Therefore, it is thought that the results of this study can easily be extended to the biomechanics of human ligaments.

Knowing the average initial length and cross sectional area of human ligaments would give the analyst, using the model presented here, enough information to predict the failure load and stress of human ligaments under certain strain conditions.

5. Conclusion

This study significantly improves the understanding of ligament failure mechanics in conditions consistent with high speed frontal automotive collisions. It has been shown the predominate mode of failure under these conditions is tibial avulsion. However mid-substance failure is still a concern. In either case, the failure: load, stress and strain all increase as the strain rate or, in the case of a frontal collision, impact velocity, increases. Further a significant correlation between ratios of geometric parameters of the ligament and the failure load and stress were identified. The recognition of these important ratios enabled the development of a reliable predictive equation for the failure load and stress.

The models developed here provide extremely important information regarding occupant injury potential in high speed frontal automotive collisions. The failure load and stress model equations may be integrated into simulation programs and used to improve automotive safety. However, to accomplish this, the results of this study must be related to the failure properties of KTH ligaments of humans. To achieve this, testing must be conducting using other porcine ligaments as well as cadaveric ligaments. Nevertheless, this study provides a solid foundation and invaluable information for further developing a model equation for the failure load and stress of all human KTH ligaments.

References

1. Kuppa S. "An Overview of Knee-Thigh-Hip Injuries in Frontal Crashes in the Unites States". *NHTSA* 2003, Paper No. 416

2. Xerogeanes JW, Fox RJ, et al. "A Functional Comparison of Animal Anterior Cruciate Ligament Models to the Human Anterior Cruciate Ligament". *Annals of Biomedical Engineering* 1998. 26:345-352.

3. Bonifasi C. "Multiaxial Viscoelastic Properties of Human Medial Collateral Ligament," MS Thesis, University of Utah, Department of Bioengineering: Spring 2003.

4. Crisco JJ, Moore DC, McGovern RD. "Strain-Rate Sensitivity of the Rabbit MCL Diminishes at Traumatic Loading Rates". *Journal of Biomechanics* 2002; 35:1379-85

5. France EP, Paulos LE, Abbott PJ, et al. "Failure Characteristics of the Medial Collateral Ligament of the Knee: Effect of High Strain Rate", *Aviation, Space and Environmental Medicine* 1987; 58:488.

6. Lydon C, Crisco JJ, Panjabi M, and Galloway M. "Effect of Elongation Rate on the Failure Properties of the Rabbit Anterior Cruciate Ligament". *Clinical Biomechanics* 1995; 10:428-433.

7. Noyes FR, Delucas JL, and Trovik PJ. "Biomechanics of Anterior Cruciate Ligament Failure: An Analysis of Strain-Rate Sensitivity and Mechanisms of Failure in Primates," *Journal of Bone and Joint Surgery* 1974; 56A:236-253.

8. Araszewski M. "Head, Hip and Knee Velocities of Restrained Occupants in Frontal Impacts". *Accident Reconstruction* 2003; 2003-01-0884.

References

9. Woo SL-Y. "Effects of Postmortem Storage by Freezing on Ligament Tensile Behavior". *Journal of Biomechanics* 1986; 19:399-404.

10. Yiannakopoulos AD, Kanellopoulos IA, et al. "The Symmetry of the Medial Collateral and Anterior Cruciate Ligament Properties. A Biomechanical Study in the Rat Hind Limb. *Journal of Musculoskeletal and Neuronal Interactions* 2005, 5(2):170-173.

11. Ozkaya N, Nordin M. *Fundamentals of Biomechanics: Equilibrium, Motion and Deformation* 1999. Springer.

12. Akeson WH, Woo SL-Y, Amiel D, Frank CD. "The Chemical Basis of Tissue Repair: The Biology of Ligaments". *Rehabilitation of the Injured Knee* 1984; 93-109.

13. Hawkins D. Ligament Biomechanics. *Current Issues in Biomechanics* 1993. Mark D. Ed. Grabiner. Human Kinetics Publishers, 123-150.

14. Pioletti DP, Rakotomanana LR, Benvenuti JF, Leyvraz PF. "Strain Rate Effect on the Mechanical Behavior of the Anterior Cruciate Ligament Bone Complex". *Medical Engineering & Physics* 1999; 21:95-100.

15. Crowninshield RD, and Pope MH. "The Strength and Failure Characteristics of the Rat Medial Collateral Ligament". *The Journal of Trauma* 1976; 16:99-105.

16. Woo SL-Y, Peterson RH, Ohland KJ, et al. "The Effects of Strain Rate on the Properties of the Medial Collateral Ligament in Skeletally Immature and Mature Rabbits: A Biomechanical and Histological Study". *Journal of Orthopaedic Research* 1990, 8: 712-21.

17. Martin RB, Burr DB, Sharkey NA. *Skeletal Tissue Mechanics* 1998. Springer, New York.

References

18. Mow VC, Ratcliffe A, Woo SL-Y. *Biomechanics of Diarthrodial Joints*, 1990. Springer-Verlag New York, Inc.

19. Pioletti DP, Rakotomanana LR, Benvenuti JF, Leyvraz PF. "Viscoelastic Constitutive Law in Large Deformations: Application to Human Knee Ligaments and Tendons". *Journal of Biomechanics* 1998*;* 31:753-757.

Appendix A

- Dell Inspiron 600m Laptop Computer
- Dell Latitude D820 Laptop Computer
- Data Acquisition Software: LabView 8.0
- National Instruments SCXI-1000 Chassis
- National Instruments 6024E DAQCard
- National Instruments SCXI-1531 Accelerometer Conditioner
- National Instruments SCXI-1520 Strain Gage Module
- Load Cell Terminal Block: SCXI-1314 Terminal Block
- PCB 353B12 Accelerometer
- Load Cell Central HJC-500
- Instron Dynatup 8250 Weight Impact Tester
- High Speed Camera: Redlake Imaging Motion Scope PCI-8000S
- High Speed Video Software: Redlake Motionscope PCI Version 2.21.1
- Computar TV Zoom Lense Model: M6Z 1212 12.5 -75mm F1.2
- Sintech 5/G Testing Machine, Model Number: 3132-149
- High Speed Video Lighting: Lowel Omni-Light
- Porter Cable® PTX5 Reciprocating Pneumatic Saw

Appendix B

Buckling Analysis for Bearing Rods

From Euler's equation for buckling:

$$P_{cr} = \frac{\pi^2 EI}{(kL)^2}$$

Where:

k = 0.5 for fixed ends

Therefore:

$$P_{cr} = \frac{4\pi^2 EI}{L^2}$$

For stainless steel, E =29.0 *10^6 PSI

In this application the length of the rod is 18 IN.

The cross section is circular with a 0.5 IN diameter.

Therefore:

$$I = \frac{\pi r^4}{4} = \frac{\pi(0.25)^4}{4}$$

Therefore:

$$P_{cr} = \frac{4\pi^2 (29.0 * 10^6)(\frac{\pi(0.25)^4}{4})}{18^2} = 10{,}841\text{LB}$$

The expected maximum force this part will encounter in is 2,000LB.

Therefore:

$$FOS = \frac{10{,}841}{2{,}000} = 5.4$$

Appendix B

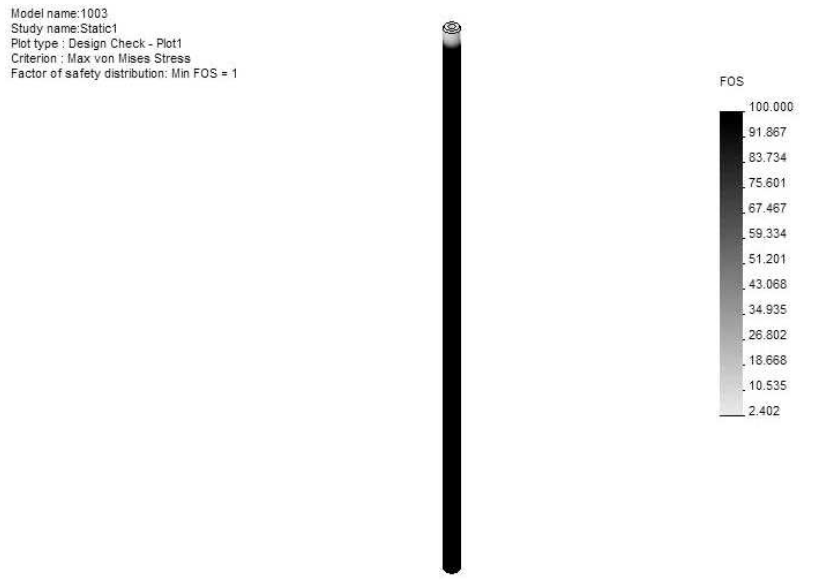

Figure A.1: Finite element stress analysis of bearing rod using cosmos

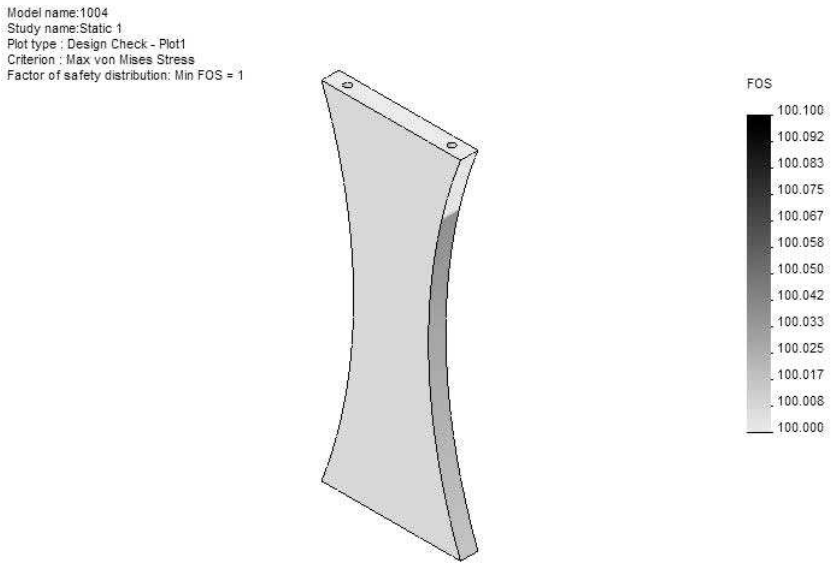

Figure A.2: Finite element tress analysis of side support using cosmos

Appendix C

Table A.1: Summary of Results for Unacceptable Tests Performed on Porcine Knee Collateral Ligaments

V_{imp} (m/s)	$\varepsilon_{failure}$ (%)	ε_{rate} (s^{-1})	σ_F (MPa)	Failure Mode	Comment
1.83	48%	26	85	Femur Broke at Gripping Bolt	Bone Disease
1.99	40%	67	15	Tibial or Fibular Avulsion	Improper Gripping
2.27	23%	35	110	Tibial or Fibular Avulsion	Improper Gripping
2.43	29%	90	61	Femur Broke at Gripping Bolt	Improper Gripping
2.83	28%	70	22	Tibial or Fibular Avulsion	Bone Disease
2.80	30%	89	67	Femur Broke at Gripping Bolt	N/A
2.82	46%	37	81	Bone Broke Around Gripping Screw	Improper Gripping
2.82	38%	81	37	Tibial Avulsion	Improper Gripping
2.95	34%	103	17	Bony Femoral Avulsion	N/A
2.89	30%	120	19	Bone Failure	Improper Gripping
3.50	31%	95	23	Tibial or Fibular Avulsion	Improper Gripping
4.46	28%	149	29	Bone Broke Around Gripping Screw	Improper Gripping

Appendix D

```
<< Statistics`LinearRegression`
<< Statistics`NonlinearFit`
DATA = Import["data.txt", "table"];
DATA2 = Import["data2.txt", "table"];
```

$$\text{NonlinearRegress}\left[\text{DATA},\ \sigma_o\left(\text{b (LoA)} + \left(\frac{\text{sr}}{\text{c}}\right)^{\frac{1}{\text{p}}}\right),\ \{\text{sr, LoA}\},\ \{\sigma_o, \text{b, c, p}\},\right.$$
$$\left.\text{RegressionReport} \to \{\text{ParameterTable},\ \text{FitResiduals, SinglePredictionCITable}\}\right]$$

$\{\text{ParameterTable} \to$

	Estimate	Asymp. SE	TStat	PValue
σ_o	6.01417	1.43227	4.19905	0.00404034
b	1.11455	0.797941	1.39678	0.205167
c	0.784295	4.68505	0.167404	0.871786
p	2.54876	3.11426	0.818417	0.440087

$,$

$\text{FitResiduals} \to \{11.3229, 5.21534, 5.09734, -14.7403, 11.5017, -21.0993, 4.97066, 7.49286, 3.43138, -23.0742, 9.93221\},$

$\text{SinglePredictionCITable} \to$

Observed	Predicted	Asymptotic SE	CI
85.53	74.2071	18.4228	{30.644, 117.77}
62.3	57.0847	16.9589	{16.9831, 97.1862}
89.07	83.9727	19.3279	{38.2695, 129.676}
51.11	65.8503	17.9931	{23.3035, 108.397}
62.41	50.9083	18.8816	{6.26033, 95.5562}
47.27	68.3693	16.4184	{29.5461, 107.193}
70.07	65.0993	16.3825	{26.3609, 103.838}
70.96	63.4671	16.973	{23.3324, 103.602}
58.95	55.5186	18.035	{12.8725, 98.1647}
39.52	62.5942	16.9148	{22.597, 102.592}
82.04	72.1078	16.7757	{32.4397, 111.776}

$\}$

Appendix D

$$\text{NonlinearRegress}\left[\text{DATA2},\ \sigma_o\left(1+\left(\frac{s}{c}\right)^{\frac{1}{p}}\right),\ \{s\},\ \{\sigma_o, c, p\},\right.$$
$$\left.\text{RegressionReport} \to \{\text{ParameterTable},\ \text{FitResiduals},\ \text{SinglePredictionCITable}\}\right]$$

$\{\text{ParameterTable} \to$

	Estimate	Asymp. SE	TStat	PValue
σ_o	29.7108	16747.8	0.00177401	0.998628
c	14.7163	174990.	0.0000840981	0.999935’
p	10.6141	5041.69	0.00210527	0.998372

$\text{FitResiduals} \to \{21.7531, -3.14764, 22.6657, -12.3241, -1.2754, -17.9129, 4.18788, 4.51589, -7.61464, -26.8464, 15.9896\},$

$\text{SinglePredictionCITable} \to$

Observed	Predicted	Asymptotic SE	CI
85.53	63.7769	20.0862	{17.4581, 110.096}
62.3	65.4476	20.4756	{18.2309, 112.664}
89.07	66.4043	19.5227	{21.385, 111.424}
51.11	63.4341	21.763	{13.2484, 113.62}
62.41	63.6854	20.318	{16.8319, 110.539}
47.27	65.1829	21.0029	{16.7501, 113.616}
70.07	65.8821	19.3203	{21.3295, 110.435}
70.96	66.4441	19.7139	{20.9837, 111.905}
58.95	66.5646	20.5027	{19.2853, 113.844}
39.52	66.3664	19.3702	{21.6987, 111.034}
82.04	66.0504	19.0337	{22.1586, 109.942}

$\}$

Appendix D

$$\text{NonlinearRegress}\left[\text{DATA},\ \sigma_o\left(1+\left(\frac{s+\text{LoA}}{c}\right)^{\frac{1}{p}}\right),\ \{s, \text{LoA}\}, \{\sigma_o, c, p\},\right.$$
$$\left.\text{RegressionReport} \to \{\text{ParameterTable},\ \text{FitResiduals}, \text{SinglePredictionCITable}\}\right]$$

$\{\text{ParameterTable} \to$

	Estimate	Asymp. SE	TStat	PValue
σ_o	30.4213	9515.37	0.00319707	0.997527
c	37.1896	175617.	0.000211765	0.999836’
p	7.57206	2092.32	0.00361897	0.997201

$\text{FitResiduals} \to \{22.1051, -3.09425, 22.2715, -11.8208, -0.675465, -17.8557, 4.057, 4.21147, -7.92071, -27.1204, 15.7669\},$

$\text{SinglePredictionCITable} \to$

Observed	Predicted	Asymptotic SE	CI
85.53	63.4249	19.9385	{17.4466, 109.403}
62.3	65.3943	20.5288	{18.0547, 112.734}
89.07	66.7985	19.8248	{21.0824, 112.514}
51.11	62.9308	21.4654	{13.4315, 112.43}
62.41	63.0855	20.6943	{15.3643, 110.807}
47.27	65.1257	20.9	{16.9302, 113.321}
70.07	66.013	19.3118	{21.4799, 110.546}
70.96	66.7485	19.6203	{21.504, 111.993}
58.95	66.8707	20.1767	{20.3431, 113.398}
39.52	66.6404	19.28	{22.1807, 111.1}
82.04	66.2731	18.9857	{22.4921, 110.054}

Appendix D

$$\text{NonlinearRegress}\left[\text{DATA},\ \sigma_o\left(1+\left(\frac{s}{c}\right)^{\frac{1}{p}}\right)+b*\text{LoA},\ \{s,\ \text{LoA}\},\ \{\sigma_o,\ b,\ c,\ p\},\right.$$

$$\left.\text{RegressionReport}\rightarrow\{\text{ParameterTable},\ \text{FitResiduals},\ \text{SinglePredictionCITable}\}\right]$$

$\{\text{ParameterTable}\rightarrow$

	Estimate	Asymp. SE	TStat	PValue
σ_o	31.2676	31.2494	1.00058	0.350353
b	6.71519	3.57475	1.8785	0.102391,
c	191.935	136.42	1.40693	0.202261
p	0.447857	1.71211	0.261582	0.801173

$\text{FitResiduals}\rightarrow\{10.9822, 6.87238, 4.48186, -15.9027, 10.9879, -19.4154, 6.06559, 6.73043, 2.06985, -23.4839, 10.6119\},$

$\text{SinglePredictionCITable}\rightarrow$

Observed	Predicted	Asymptotic SE	CI
85.53	74.5478	18.5006	{30.8008, 118.295}
62.3	55.4276	18.437	{11.831, 99.0243}
89.07	84.5881	19.4756	{38.5357, 130.641}
51.11	67.0127	18.4687	{23.3412, 110.684}
62.41	51.4221	18.9648	{6.57757, 96.2667}
47.27	66.6854	17.7346	{24.7497, 108.621}
70.07	64.0044	17.2301	{23.2617, 104.747}
70.96	64.2296	17.269	{23.3949, 105.064}
58.95	56.8802	19.1603	{11.5732, 102.187}
39.52	63.0039	16.9435	{22.9389, 103.069}
82.04	71.4281	17.1232	{30.9383, 111.918}

$\}$